Model characterization and dark matter in the secluded $U(1)'$ model

Yaşar Hiçyılmaz,[1,2,*] Levent Selbuz,[3,†] Levent Solmaz,[1,‡] and Cem Salih Ün[4,5,§]

[1]*Department of Physics, Balıkesir University, TR10145 Balıkesir, Turkey*
[2]*School of Physics & Astronomy, University of Southampton, Highfield, Southampton SO17 1BJ, United Kingdom*
[3]*Department of Engineering Physics, Ankara University, TR06100 Ankara, Turkey*
[4]*Department of Physics, Bursa Uludağ University, TR16059 Bursa, Turkey*
[5]*Departamento de Ciencias Integradas y Centro de Estudios Avanzados en Física Matemáticas y Computación, Campus del Carmen, Universidad de Huelva, Huelva 21071, Spain*

(Received 29 November 2021; accepted 8 March 2022; published 29 March 2022)

We consider a class of $U(1)'$-extended minimal supersymmetric extension of the Standard Model (MSSM) in which the $U(1)'$ symmetry is broken by vacuum expectation values of four MSSM singlet fields. While one MSSM singlet field interacts with the MSSM Higgs fields, three of them interact only with each other in forming a secluded sector. Assigning universal $U(1)'$ charges for three families, the anomaly cancellation condition requires exotic fields which are assumed to be heavy and decoupled. We discuss a variety of $U(1)'$ charge assignments and anomaly cancellation, Z'/Z hierarchy, neutralinos, charginos and the Higgs sector. We find that the typical spectra involve two CP-odd Higgs bosons lighter than about 200 GeV and 600 GeV respectively, which are mostly formed by the MSSM singlet fields. If the relic density of dark matter is saturated only by a neutralino, compatible solutions predict LSP neutralinos formed by the MSSM singlet fields in the mass scales below about 600 GeV, while it is possible to realize MSSM neutralino LSP above these mass scales. One can classify the implications in three scenarios. Scenario I involves NLSP charginos, while Scenario II involves charginos which do not participate coannihilation processes with the LSP neutralino. These two scenarios predict MSSM singlet LSP neutralinos, while Scenario I leads to larger scattering cross sections of dark matter. Scenario III has the solutions in which the MSSM neutralinos are considerably involved in LSP decomposition which yields very large scattering cross section excluded by the direct detection experiments.

DOI: 10.1103/PhysRevD.105.055029

I. INTRODUCTION

Despite the lack of any direct signal of new physics beyond the Standard Model (SM), the minimal supersymmetric extension of the Standard Model (MSSM) is still one of the forefront candidates because of the motivation of resolution to the gauge hierarchy problem [1–5], stability of the Higgs potential [6–11], pleasant candidates for the dark matter, with an additional attraction from the gauge coupling unification at the grand unification theory (GUT) scale ($M_{\mathrm{GUT}} \simeq 2.4 \times 10^{16}$ GeV). On the other hand, the lack of a direct signal might point to a deviation from the minimal point of view in constructing models beyond the SM. For instance, if the lightest supersymmetric particle (LSP) is not a mixture of MSSM neutralinos [12–14], many of the signal processes currently under the collider analyses may not be available at the collision energies of today. A similar discussion can be followed also for the null results from the dark matter experiments [15–17].

In addition to the current results from the experiments, possible resolutions to some long standing problems such as absence of the right-handed neutrinos and the μ problem in MSSM [18] can motivate us to construct models beyond the SM which extends the particle content and/or symmetrical structure of the MSSM. In this context, a larger symmetry group which supplements the MSSM gauge group with an extra $U(1)'$ can address the resolution to the μ problem. If the extra $U(1)'$ symmetry is imposed in a way that the MSSM fields are also nontrivially charged under it, the $\mu H_d H_u$ is not allowed in the superpotential due to the gauge invariance under $U(1)'$. On the other hand, it can be generated effectively through the vacuum expectation value (VEV) of a field S, which is preferably singlet under the

*yasarhicyilmaz@balikesir.edu.tr
†selbuz@eng.ankara.edu.tr
‡lsolmaz@balikesir.edu.tr
§cemsalihun@uludag.edu.tr

MSSM gauge symmetry so that its VEV breaks only the $U(1)'$ symmetry. In this case the superpotential involves a term such as SH_uH_d, and through the $U(1)'$ breaking, the μ term is generated effectively as $\mu_{\rm eff} \sim \mathcal{O}(\langle S \rangle)$ [19–28]. In this way, the radiative electroweak symmetry breaking (REWSB) is linked to the $U(1)'$ symmetry breaking through the renormalization group equations (RGEs). Such an extension can still be considered to be minimal, and it is well motivated in superstring theories [29], grand unified theories [30], and in dynamical electroweak breaking theories [31].

In addition to extending the symmetry, the $U(1)'$ models also extend the particle content of MSSM by adding Z'—the gauge boson associated with the $U(1)'$ group and the right-handed neutrinos. The right-handed neutrinos can be considered to complete the representations of matter field families so that the model can be embedded in a larger GUT group such as E_6. Besides, the right-handed neutrinos contribute to the anomaly cancellations, and they can provide a natural framework to implement seesaw mechanisms [32] for nonzero neutrino masses and mixing [33]. In this context, $\langle S \rangle$ significantly contributes to the right-handed sneutrino and Z' masses as well as their superpartners. However, the presence of a neutral gauge boson Z' brings a strong impact on this class of models, since the current experimental results exclude the solutions with $M_{Z'} \lesssim 4$ TeV. Such a strong exclusion results in a $U(1)'$ breaking scale at the order of $\mathcal{O}(10$ TeV$)$ and consequently $\mu_{\rm eff} \sim$ a few TeV, which softly brings the μ problem back to the $U(1)'$ models, even though a resolution to the naturalness problem can be accommodated [34]. Note that this strong bound can be avoid if the gauge coupling of $U(1)'$ is significantly small ($\lesssim 10^{-5}$) [35–37], or negligibly couple to the fermions of the first to families [38,39]. However, these conditions on the couplings cannot be met if the gauge coupling unification is imposed at $M_{\rm GUT}$ and/or the family universal $U(1)'$ charges are assumed. On the other hand, if the $U(1)'$ symmetry breaking involves three more MSSM singlet fields (S_1, S_2, S_3) [40,41], a μ term at the order of electroweak symmetry breaking can be realized, while Z' remains heavy to be consistent with the current experimental results. These three MSSM singlet fields form the secluded sector, and their number can be determined by considering the physical properties of vacua of the scalar potential. The minimal setup of $U(1)$ extended supersymmetric models ($\kappa \to 0$ in $\kappa/3 S_1 S_2 S_3$), the unstable vacua of the scalar potentials can be avoided by setting the $U(1)'$ breaking scale very large ($\mathcal{O}(10$ TeV$)$), which leads to a heavy S field and its neutralino. In these cases, the testable low scale implications of $U(1)'$ models are not distinguishable from the MSSM implications [42–44]. Even though extending the scalar sectors with one or two more MSSM singlet fields can allow a relatively lower breaking scale for $U(1)'$ symmetry, the requirement of physical vacua is still effective, since the solutions in such frameworks can still yield vanishing VEVs for the MSSM Higgs fields or $v_s \sim v_u \sim v_d$, which also cancels the $Z' - Z$ hierarchy [40]. In this context, the minimal form of the secluded sector can be spanned by three MSSM singlet fields. Of course it could include more fields; however, their effects can still be taken into account with three fields by varying the relevant couplings (λ and κ) and VEVs (v_S and v_i).

We refer to the class of supersymmetric $U(1)'$ models with three additional MSSM singlet fields as the secluded $U(1)'$ model [40,41,45,46]. Even though we allow that the additional $U(1)'$ symmetry can be broken at a scale of order multi-TeV [$\mathcal{O}(10)$ TeV], we assume $U(1)$-extended MSSM emerges at $M_{\rm GUT}$ resulting from the breaking of a larger gauge symmetry such as E_6. We perform random scans by imposing boundary conditions on the GUT scale parameters at $M_{\rm GUT}$, which is spanned by the universal soft supersymmetry breaking (SSB) mass terms for the supersymmetric scalars and gauginos. Note that the SSB masses of the Higgs fields are calculated by minimizing the superpotential, and in general, it implies nonuniversal SSB masses for the MSSM Higgs fields. Since the breaking scale of $U(1)'$ is unknown, the set of the free parameters in secluded $U(1)'$ model involves VEVs of the MSSM singlet scalar fields. The rest of the paper is organized as follows: We first briefly review the secluded $U(1)'$ models in Sec. II with its superpotential, particle content, nontrivial $U(1)'$ charges of the fields and anomaly cancellations, as well as the field content and the physical mass states. After we describe the scanning procedure and summarize the relevant experimental constraints in Sec. III, we present and discuss the LHC and dark matter implications of the model in Sec. IV. Finally, we conclude our findings in Sec. V.

II. THE SECLUDED $U(1)'$ MODEL

In this section we present the relevant ingredient and some salient features of the secluded $U(1)'$ model, which is based on the gauge group $SU(3)_c \times SU(2)_L \times U(1)_Y \times U(1)'$. Such an extension of the MSSM gauge group can emerge in the grand unified theories based on a gauge group larger than $SU(5)$ such as $SO(10)$ [47–50] and/or E_6 [51–54]. In the common convention the $U(1)'$ extension of MSSM results from the E_6 through the following cascade of the symmetry breakings,

$$\begin{aligned} E_6 &\to SO(10) \times U(1)_\psi \\ &\to SU(5) \times U(1)_\chi \times U(1)_\psi \\ &\to SU(3)_C \times SU(2)_L \times U(1)_Y \times U(1)', \end{aligned} \tag{1}$$

where $U(1)'$ group at the end of the breaking chain is, in principle, a linear combination of $U(1)_\chi$ and $U(1)_\psi$ with charge $Q' = Q_\chi \cos\theta_{E_6} + Q_\psi \sin\theta_{E_6}$. On the other hand, a general configuration of the $U(1)'$ charges cannot be restricted to these two classes of the $U(1)'$ models [23,39,55–58]. A general set of equations for the charges

can be obtained from the anomaly cancellation condition, and these conditions also depend on the exotic fields involved in the model. In our work, we consider the following superpotential,

$$\hat{W} = W_{\rm MSSM}(\mu = 0) + \lambda \hat{S}\hat{H}_u \cdot \hat{H}_d + h_\nu \hat{L} \cdot \hat{H}_u \hat{N} + \frac{\kappa}{3}\hat{S}_1\hat{S}_2\hat{S}_3 + \sum_{i=1}^{n_{\mathcal{Q}}} h_Q^i \hat{S}\hat{\mathcal{Q}}_i\hat{\bar{\mathcal{Q}}}_i + \sum_{j=1}^{n_{\mathcal{L}}} h_L^j \hat{S}\hat{\mathcal{L}}_j\hat{\bar{\mathcal{L}}}_j, \quad (2)$$

where the matter superfields of the MSSM corresponding to the squarks and sleptons $\hat{Q}, \hat{U}, \hat{D}, \hat{L}$, and $\hat{E}$ are included in $W_{\rm MSSM}$, and $\hat{H}_u, \hat{H}_d$ are the MSSM Higgs doublets. The new ingredient from the $U(1)'$ inclusion can be listed as the MSSM singlet scalars $S, S_{1,2,3}$, right-handed neutrino superfield $\hat{N}$ and exotic fields $\mathcal{Q}_i$, $\mathcal{L}_i$. In addition, the model includes a neutral gauge boson associated with the $U(1)'$ symmetry and its supersymmetric partner. Note that we do not assume $Q'_{H_u} + Q'_{H_d} = 0$ in our scans. In this case, the gauge invariance forbids the bilinear mixing ($\mu \hat{H}_u \hat{H}_d$) in the MSSM superpotential, which is stated as $W_{\rm MSSM}(\mu = 0)$ in Eq. (2). It is generated effectively through the VEV of S so that $\mu_{\rm eff} \equiv \lambda \langle S \rangle$. However, the emergence of such an effective term induces mixed anomalies between $U(1)'$ and the MSSM gauge group; cancellation of such anomalies also requires exotic fields in the particle spectrum, and the anomaly cancellation can be maintained by introducing exotic fields, which are vectorlike with respect to MSSM, but chiral under the $U(1)'$ group.

If a general $U(1)'$ charge assignments is as shown in Table I, the gauge invariance condition yields the following equations,

$$\begin{aligned}
0 &= Q'_S + Q'_{H_u} + Q'_{H_d}, \\
0 &= Q'_Q + Q'_{H_u} + Q'_U, \\
0 &= Q'_Q + Q'_{H_d} + Q'_D, \\
0 &= Q'_L + Q'_{H_d} + Q'_E, \\
0 &= Q'_{\mathcal{Q}} + Q'_{\bar{\mathcal{Q}}} + Q'_S, \\
0 &= Q'_{\mathcal{L}} + Q'_{\bar{\mathcal{L}}} + Q'_S, \\
0 &= Q'_L + Q'_{H_u} + Q'_N, \\
0 &= Q'_{S_1} + Q'_{S_2} + Q'_{S_3}.
\end{aligned} \quad (3)$$

Note that if a special configuration with $Q'_S = 0$ can be found, the μ term becomes allowed by the gauge invariance. However, a consistent $Z - Z'$ mass hierarchy and mixing require nonzero $U(1)'$ charges for all MSSM singlet scalar fields $S, S_{1,2,3}$. Another set of conditions for the charges is obtained from the vanishing $U(1)' - SU(3)_c - SU(3)_c$, $U(1)' - SU(2)_L - SU(2)_L$, $U(1)' - U(1)_Y - U(1)_Y$, $U(1)'$ – graviton – graviton, $U(1)' - U(1)' - U(1)_Y$ and $U(1)' - U(1)' - U(1)'$ anomalies, as follows:

$$0 = 3(2Q'_Q + Q'_U + Q'_D) + n_{\mathcal{Q}}(Q'_{\mathcal{Q}} + Q'_{\bar{\mathcal{Q}}}), \quad (4)$$

$$0 = 3(3Q'_Q + Q'_L) + Q'_{H_d} + Q'_{H_u}, \quad (5)$$

$$0 = 3\left(\frac{1}{6}Q'_Q + \frac{1}{3}Q'_D + \frac{4}{3}Q'_U + \frac{1}{2}Q'_L + Q'_E\right) + \frac{1}{2}(Q'_{H_d} + Q'_{H_u}) + 3n_{\mathcal{Q}}Y^2_{\mathcal{Q}}(Q'_{\mathcal{Q}} + Q'_{\bar{\mathcal{Q}}}) + n_{\mathcal{L}}Y^2_{\mathcal{L}}(Q'_{\mathcal{L}} + Q'_{\bar{\mathcal{L}}}), \quad (6)$$

$$0 = 3(6Q'_Q + 3Q'_U + 3Q'_D + 2Q'_L + Q'_E + Q'_N) + 2Q'_{H_d} + 2Q'_{H_u} + Q'_S + Q'_{S_1} + Q'_{S_2} + Q'_{S_3} + 3n_{\mathcal{Q}}(Q'_{\mathcal{Q}} + Q'_{\bar{\mathcal{Q}}}) + n_{\mathcal{L}}(Q'_{\mathcal{L}} + Q'_{\bar{\mathcal{L}}}), \quad (7)$$

$$0 = 3(Q'^2_Q + Q'^2_D - 2Q'^2_U - Q'^2_L + Q'^2_E) - Q'^2_{H_d} + Q'^2_{H_u} + 3n_{\mathcal{Q}}Y_{\mathcal{Q}}(Q'^2_{\mathcal{Q}} - Q'^2_{\bar{\mathcal{Q}}}) + n_{\mathcal{L}}Y_{\mathcal{L}}(Q'^2_{\mathcal{L}} - Q'^2_{\bar{\mathcal{L}}}), \quad (8)$$

$$0 = 3(6Q'^3_Q + 3Q'^3_D + 3Q'^3_U + 2Q'^3_L + Q'^3_E + Q'^3_N) + 2Q'^3_{H_d} + 2Q'^3_{H_u} + Q'^3_S + Q'^3_{S_1} + Q'^3_{S_2} + Q'^3_{S_3} + 3n_{\mathcal{Q}}(Q'^3_{\mathcal{Q}} + Q'^3_{\bar{\mathcal{Q}}}) + n_{\mathcal{L}}(Q'^3_{\mathcal{L}} + Q'^3_{\bar{\mathcal{L}}}). \quad (9)$$

All these conditions from the gauge invariance and the anomaly cancellations should be satisfied for particular pattern of charges and parameters, which requires the number of exotics. Based on the choice of exotics in the model, one of the simplest solution to the mixed anomaly constraints requires $n_{\mathcal{Q}} = 3$ color triplets with $Y_{\mathcal{Q}} = -1/3$, and $n_{\mathcal{L}} = 2$ color singlets with $Y_{\mathcal{L}} = -1$. Recall that these exotic fields are singlets under $SU(2)_L$ as mentioned before and listed in Table I. In our analyses, we assume the exotics to be very heavy and decouple from the low-scale spectrum. In this sense, their charges are considered only for the anomaly cancellation in our work.

A. Gauge Boson Masses and Mixing

As mentioned before the model introduces a new neutral gauge boson Z' and its superpartner $\tilde{B}'$ associated with the gauged $U(1)'$ symmetry. The symmetry breaking in this model being realized is very similar to the Higgs mechanism, but in this case, the electroweak and $U(1)'$ symmetry breaking are correlated. The fields developing nonzero VEVs during the symmetry breaking, $SU(2)_L \times U(1)_Y \times U(1)' \to U(1)_{\rm EM}$, can be listed as follows:

$$\langle H_u \rangle = \frac{1}{\sqrt{2}}\begin{pmatrix} 0 \\ v_u \end{pmatrix}, \qquad \langle H_d \rangle = \frac{1}{\sqrt{2}}\begin{pmatrix} 0 \\ v_d \end{pmatrix}, \qquad \langle S \rangle = \frac{v_S}{\sqrt{2}}, \qquad \langle S_i \rangle = \frac{v_{S_i}}{\sqrt{2}}. \quad (10)$$

TABLE I. Gauge quantum numbers of quark ($\hat{Q}, \hat{U}, \hat{D}$), lepton ($\hat{L}, \hat{N}, \hat{E}$), Higgs ($\hat{H}_u, \hat{H}_d$), MSSM-singlet ($\hat{S}, \hat{S}_1, \hat{S}_2, \hat{S}_3$), exotic quark ($\hat{\mathcal{Q}}, \hat{\bar{\mathcal{Q}}}$) and exotic lepton ($\hat{\mathcal{L}}, \hat{\bar{\mathcal{L}}}$) superfields.

Field	$\hat{Q}$	$\hat{U}$	$\hat{D}$	$\hat{L}$	$\hat{N}$	$\hat{E}$	$\hat{H}_u$	$\hat{H}_d$	$\hat{S}$	$\hat{S_1}$	$\hat{S_2}$	$\hat{S_3}$	$\hat{\mathcal{Q}}$	$\hat{\bar{\mathcal{Q}}}$	$\hat{\mathcal{L}}$	$\hat{\bar{\mathcal{L}}}$
$SU(3)_C$	3	$\bar{3}$	$\bar{3}$	1	1	1	1	1	1	1	1	1	3	$\bar{3}$	1	1
$SU(2)_L$	2	1	1	2	1	1	2	2	1	1	1	1	1	1	1	1
$U(1)_Y$	1/6	−2/3	1/3	−1/2	0	1	1/2	−1/2	0	0	0	0	$Y_{\mathcal{Q}}$	$-Y_{\mathcal{Q}}$	$Y_{\mathcal{L}}$	$-Y_{\mathcal{L}}$
$U(1)'$	Q'_Q	Q'_U	Q'_D	Q'_L	Q'_N	Q'_E	Q'_{H_u}	Q'_{H_d}	Q'_S	Q'_{S_1}	Q'_{S_2}	Q'_{S_3}	$Q'_{\mathcal{Q}}$	$Q'_{\bar{\mathcal{Q}}}$	$Q'_{\mathcal{L}}$	$Q'_{\bar{\mathcal{L}}}$

Since $S, S_{1,2,3}$ fields are singlet under the MSSM gauge group, the W and Z bosons acquire their masses through the VEVs of H_u and H_d as in the usual electroweak symmetry breaking; thus, the condition $v_u^2 + v_d^2 = v_{\rm SM}^2$ should still hold in this model. On the other hand, because of the nontrivial charges of all the superfields under $U(1)'$ as listed in Table I, the Z' boson receives its mass from all the VEVs. In this case, since v_S and/or v_{S_i} are expected to be much greater than v_u and v_d, the secluded sector can be accounted for as the main source of the Z' mass. However, apart from the mass acquisition, nontrivial H_u and H_d charges induce a nonzero mixing between Z and Z' associated with their mass-square matrix,

$$M^2_{ZZ'} = \begin{pmatrix} M_Z^2 & \Delta^2 \\ \Delta^2 & M_{Z'}^2 \end{pmatrix}, \tag{11}$$

written in (Z, Z') basis in terms of

$$\begin{aligned} M_Z^2 &= \frac{1}{4}(g_1^2 + g_2^2)(v_u^2 + v_d^2), \\ M_{Z'}^2 &= g_1'^2\left(Q'^2_{H_u} v_u^2 + Q'^2_{H_d} v_d^2 + Q'^2_S v_S^2 + \sum_{i=1}^{3} Q'^2_{S_i} v_{S_i}^2\right), \\ \Delta^2 &= \frac{1}{2}\sqrt{g_1^2 + g_2^2}\, g_1'(Q'^2_{H_u} v_u^2 - Q'^2_{H_d} v_d^2). \end{aligned} \tag{12}$$

Diagonalizing the mass-square matrix in Eq. (11) yields the following mixing angle between Z and Z',

$$\theta_{ZZ'} = \frac{1}{2}\arctan\left(\frac{2\Delta^2}{M_{Z'}^2 - M_Z^2}\right), \tag{13}$$

and the electroweak precision data strongly bounds the $Z - Z'$ mixing angle as $\theta_{ZZ'} \lesssim 10^{-3}$ [59–61]. Applying such a strict constraint to the mixing between Z and Z' allows only solutions with the following properties:

(1) $g_1' \ll g_1$.
(2) $M_{Z'} \gg M_Z$.
(3) $Q'_{H_d}/Q'_{H_u} \simeq v_u/v_d \equiv \tan\beta$.

The first two conditions separately bring a naive application of the large electron-positron collider (LEP) two bound on $M_{Z'}$ as $M_{Z'}/g_1' \geq 6$ TeV [62]. The first condition cannot be realized when the secluded model is constrained by the gauge coupling unification at $M_{\rm GUT}$, since the gauge coupling unification yields $g_1' \sim g_1, g_2$ at the low scale. Thus, a consistent $Z - Z'$ mixing with the precision data can be satisfied by spectra involving heavy Z'. Alternatively, one can apply the third condition by adjusting Q'_{H_u} and Q'_{H_d}; however, since it enhances the model dependency in the results, we do not consider it in our study.

Note that the gauge invariance also allows a tree-level mixing between the gauge bosons of two Abelian gauge groups through $\xi B^{\mu\nu} B'_{\mu\nu}$, where $B_{\mu\nu}$ and $B'_{\mu\nu}$ correspond to the field-strength tensors for $U(1)_Y$ and $U(1)'$ in our work respectively. This term leads to a gauge-covariant derivative in a noncanonical form [63,64], which also induces tree-level mixing between the MSSM Higgs fields and MSSM singlet scalar fields of the secluded sector. It also induces a mixing between the photon and Z' in addition to $Z - Z'$ mixing, which alters the mixing angle given in Eq. (2.13) such that the physical mass states of the gauge bosons involve a massless photon [65,66]. Even though the gauge kinetic mixing can yield relatively lighter Z' in the mass spectrum [67], it is severely bounded from above. The analyses over the LEP data yields an upper bound on the gauge kinetic mixing as $\xi \lesssim 2.5 \times 10^{-3}$ [59], and the current collider analyses have upgraded this bound as $\xi \lesssim 3 \times 10^{-4}$ from searches over different decay modes of Z' [68–70]. In addition, the direct detection experiments can severely restrict the gauge kinetic mixing through the scattering of DM, since it raises the photon and Z-boson abundance [71], unless the scattering is not sufficiently suppressed by the Z' mass. Thus, the gauge kinetic mixing does not loosen the severe bound on the Z' mass which is also required by the resonance searches of the collider analyses [72,73]. In this context, we assume the available spectra in our model involve heavy Z', and we set the gauge kinetic mixing to zero, since its impact would be negligible after imposing the relevant constraints on it.

B. Neutralinos and charginos

Depending on the hypercharges of the exotic fields ($\mathcal{Q}$ and $\mathcal{L}$), the secluded $U(1)'$ model extends both the charged and neutral sectors of MSSM. Their interference enriches the phenomenology such as lowering the mass bound on Z' [67,74], triggering $U(1)'$ breaking by

guaranteeing negative m_S^2 [19] etc. Even though it is possible to have exotic fields coupling the quarks to leptons depending on baryon and lepton numbers [75], in the standard configuration they can couple only to quarks or leptons. Besides, it is possible to configure the $U(1)'$ charges in which the exotics are allowed to couple only to S field at tree level. In this case, $SU(3)$ triplet exotic field $\mathcal{Q}$ is still allowed to be produced at the collider experiments; thus, the resonance searches are still able to bound their masses as $m_{\tilde{Q}} \gtrsim 5$ TeV [76]. In this context, we assume the exotics can couple only to the MSSM singlet S field, and they are heavy. Thus, their observable effects at the low scale become suppressed, while they are still effective in $U(1)'$ symmetry-breaking, anomaly cancellation etc.

Assuming the exotic fields to be decoupled at a high scale, only the MSSM singlet fields can be involved in the spectrum, and the neutral sector of this class of secluded $U(1)'$ models significantly extends the neutralinos with $\tilde{S}, \tilde{B}', \tilde{S}_{1,2,3}$. After the $U(1)'$ and electroweak symmetry breakings, these neutralinos together with the MSSM neutralinos mix each other, and the resultant mass matrix for the neutralino sector can be obtained in the usual basis ordered as $(\tilde{B}, \tilde{W}, \tilde{H}_d, \tilde{H}_u, \tilde{S}, \tilde{B}', \tilde{S}_1, \tilde{S}_2, \tilde{S}_3)$ as follows:

$$M_{\tilde{\chi}} = \left(\begin{array}{cccc|ccccc} & & & & 0 & M_{BB'} & 0 & 0 & 0 \\ & & & & 0 & 0 & 0 & 0 & 0 \\ & \text{MSSM}(\mu=\mu_{\text{eff}}) & & & -\frac{\lambda v_u}{2} & g_1' Q'_{H_d} v_d & 0 & 0 & 0 \\ & & & & -\frac{\lambda v_d}{2} & g_1' Q'_{H_u} v_u & 0 & 0 & 0 \\ \hline 0 & 0 & -\frac{\lambda v_u}{2} & -\frac{\lambda v_d}{2} & 0 & g_1' Q'_S v_S & 0 & 0 & 0 \\ M_{BB'} & 0 & g_1' Q'_{H_d} v_d & g_1' Q'_{H_u} v_u & g_1' Q'_S v_S & M_{B'} & g_1' Q'_{S_1} v_{S_1} & g_1' Q'_{S_2} v_{S_2} & g_1' Q'_{S_3} v_{S_3} \\ 0 & 0 & 0 & 0 & 0 & g_1' Q'_{S_1} v_{S_1} & 0 & -\frac{\kappa v_{S_3}}{\sqrt{2}} & -\frac{\kappa v_{S_2}}{\sqrt{2}} \\ 0 & 0 & 0 & 0 & 0 & g_1' Q'_{S_2} v_{S_2} & -\frac{\kappa v_{S_3}}{\sqrt{2}} & 0 & \frac{\kappa v_{S_1}}{\sqrt{2}} \\ 0 & 0 & 0 & 0 & 0 & g_1' Q'_{S_2} v_{S_3} & -\frac{\kappa v_{S_2}}{\sqrt{2}} & -\frac{\kappa v_{S_1}}{\sqrt{2}} & 0 \end{array}\right) \tag{14}$$

The upper block called MSSM in the mass matrix given above represents the usual MSSM neutralinos and their mixing. However, since the μ term is not allowed at tree level and is effectively generated by the VEV of S, the secluded $U(1)'$ is effective in generating the masses of MSSM Higgsinos and interfering in the mixing of MSSM neutralinos. In addition, $\tilde{B}'$ can mix with $\tilde{B}$ through the kinetic mixing, and MSSM Higgsinos through $Z - Z'$ mixing which are quantified with $M_{BB'}$, $g_1' Q'_{H_d} v_d$, and $g_1' Q'_{H_u} v_u$ in the neutralino mass matrix, respectively. Similarly, S can mix with the MSSM Higgsinos and its mixing is proportional to its coupling to the Higgs fields as λv_d and λv_u. On the other hand, $\tilde{S}_1$, $\tilde{S}_2$, and $\tilde{S}_3$ mix only with the $U(1)'$ neutralinos, while they leave the MSSM neutralinos intact.

In addition to their effects in the neutralino sector, these fields including $\tilde{B}'$ can also escape from the experimental detection and they can easily be much lighter than the MSSM neutralinos. For instance, heavy mass bounds on gluinos as $m_{\tilde{g}} \geq 2.1$ TeV [77] also bounds the bino and wino masses at about 300 GeV and 600 GeV, respectively when the universal gaugino mass is imposed at the GUT scale (for a recent study with universal gaugino mass at the GUT scale, see Ref. [78]). In addition, the current measurements of the Planck satellite on the relic density of the dark matter can lift the mass bound up to about 1 TeV, especially when the dark matter is composed mostly by binos [17]. Even though the LHC bounds can be loosened when the LSP is formed mostly by the MSSM Higgsinos ($\mu \ll M_1, M_2$), the current null results from the direct detection experiments require $\mu \gtrsim 700$ GeV for the Higgsino-like dark matter [17,79,80]. Note that this bound is significantly reduced to about 200–300 GeV if the DM is realized to be Higgsino-bino and/or Higgsino-wino mixture [81].

As a consequence of such severe bounds on the MSSM neutralinos, the non-MSSM neutralinos can be more likely to form the LSP neutralino in the low-scale mass spectrum, and in this context they yield quite different phenomenology in both the collider and the dark matter experiments. If the LSP is formed mostly by the secluded $U(1)'$ sector, then some of the particles in the MSSM spectrum might be realized to be a long-lived state, since they do not directly couple to the LSP. Even though, the current LHC constraints on the strongly-interacting particles such as squarks and gluinos yield a consistent lifetime for these particles, it is still possible to have long-lived staus and charginos in the low-scale spectrum, and the model should be constrained to avoid possible missing electric charges from such states escaping from detectors.

On the other hand, even though the stop and gluino are not allowed to be long lived by the LHC constraints, the current bounds on these particles can be significantly modified depending on the decay of the lightest MSSM neutralino into the LSP. Since these particles do not directly couple to the LSP, their possible signal processes remain the same as those which are excessively analyzed in the collider experiments [82]. In these processes, if the lightest MSSM neutralino does not decay in the detector and it forms the missing energy, then the current constraints on the stop and the gluino still hold. On the other hand, if the lightest MSSM neutralino is allowed to decay into the LSP in the detector, then such processes can significantly modify (probably loosen) the current bounds on the stop and gluino (see Ref. [13] for the case in which stop does not directly couple to LSP).

The non-MSSM LSP also yields an interesting phenomenology in the dark matter experiments. Since S is allowed to interact with the MSSM Higgs fields at tree level, its superpartner ($\tilde{S}$) scatters at nuclei through Higgs portal. Even though its scattering cross section is expected to be rather low, such solutions will be able to be tested soon under the current and future projected sensitivity of the results from XENON experiment [83]. The scattering cross section can be further lowered when the LSP is formed by $\tilde{S}_{1,2,3}$, since they interact only with S. However, their annihilation processes can still yield interesting results for the indirect detection of dark matter and can be tested under light of the current results from FermiLAT [84,85].

Before concluding the neutralino sector in the model, we should also note the chargino sector. Since only the MSSM singlet fields can be involved in the detectable low-scale spectrum, the physical states of the chargino sector is formed by the MSSM fields such as wino and Higgsino. On the other hand, as discussed in the neutralino mass matrix, the charged Higgsino mass (μ) is determined effectively by the VEV of S, thus the secluded $U(1)'$ sector is still effective in the phenomenology of the chargino sector.

C. Higgs bosons

The presence of the MSSM singlet S and S_i fields significantly extends the Higgs boson sector of the MSSM in the secluded $U(1)'$ model. In the physical spectrum there are six CP-even Higgs bosons, while the number of the CP-odd Higgs bosons is four. In addition to the enrichment in the Higgs boson spectrum, the Higgs sector becomes more complicated through the tree-level mixing, which does not exist in the MSSM framework. The Higgs potential generated with F terms can be written as [41]

$$V_F = |\lambda|^2[|H_d H_u|^2 + |S|^2(H_d^\dagger H_d + H_u^\dagger H_u)] + \frac{|\kappa|^2}{9}(|S_1 S_2|^2 + |S_2 S_3|^2 + |S_1 S_3|^2], \tag{15}$$

where the $SU(2)_L$ indices are suppressed for simplicity. While the F terms allow mixing only among the MSSM Higgs doublets and the MSSM singlet S scalar, the other MSSM singlets can mix with the MSSM Higgs fields through the scalar potential generated by D terms, which is

$$V_D = \frac{g_1^2+g_2^2}{8}(H_d^\dagger H_d - H_u^\dagger H_u)^2 + \frac{g_2^2}{2}|H_d^\dagger H_u|^2 + \frac{g_1'^2}{2}\left(Q'_{H_d}H_d^\dagger H_d + Q'_{H_u}H_u^\dagger H_u + Q'_S|S|^2 + \sum_{i=1}^{3} Q'_S|S_i|^2\right)^2. \tag{16}$$

After all, the scalar potential generated by the F and D terms induce tree-level mixing among all the Higgs scalars. In addition, the soft supersymmetry breaking Lagrangian contributes to the Higgs phenomenology through the following terms,

$$\mathcal{L}_{\not{\text{SUSY}}} = m_{H_d}^2 H_d^\dagger H_d + m_{H_u}^2 H_u^\dagger H_u + m_S^2|S|^2 + \sum_{i=1}^{3} m_{S_i}^2|S_i|^2 - \lambda A_\lambda S H_d H_u - \frac{\kappa}{3}A_\kappa S_1 S_2 S_3 - m_{SS_1}^2 S S_1 - m_{SS_2}^2 S S_2 - m_{S_1S_2}^2 S_1^\dagger S_2. \tag{17}$$

The tree-level mass-square matrix for CP-even and CP-odd Higgs bosons is generated through the SSB masses and the vacuum expectation values defined as

$$H_d = \frac{1}{\sqrt{2}}\begin{pmatrix} v_d + h_d^0 + iA_d \\ \sqrt{2}h_d^- \end{pmatrix}, \quad H_u = \frac{1}{\sqrt{2}}\begin{pmatrix} \sqrt{2}h_u^+ \\ v_u + h_u^0 + iA_u \end{pmatrix}, \tag{17a}$$

$$S = \frac{1}{\sqrt{2}}(v_S + S + iA_S), \quad S_i = \frac{1}{\sqrt{2}}(v_{S_i} + S_i + iA_{S_i}). \tag{17b}$$

Note that the gauge boson associated with $U(1)'$ group (Z') receives its mass from the VEVs of all the scalar fields given in Eqs. (17a) and (17b); however, since $v_S, v_{S_i} \gg v_d, v_u$, the VEVs of MSSM singlet fields are dominant in Z' mass. Thus, a heavy mass bound on Z' is expected to yield a strong impact in the MSSM singlet scalar sector. In a class of $U(1)'$ extended supersymmetry models, the absence of the fields S_i results in high $U(1)'$ breaking scale ($v_S \gtrsim 10$ TeV) [34,86] to realize $M_{Z'} \geq$ 4 TeV–5 TeV [87]. In addition, the VEVs, in principle do not have to align in the same direction, so they can be also a

source for CP-violation. However, we assume the CP-conservation in our work by setting $\theta_i = 0$ (for a detailed discussion about CP-conservation and breaking, see Ref. [41]).

The scalar potentials involving the Higgs fields yield the following symmetric mass-square matrix for the CP-even Higgs fields,

$$\mathcal{M}^2_{\text{even}} = \begin{pmatrix} M^2_{11} & M^2_{12} & M^2_{13} & M^2_{14} & M^2_{15} & M^2_{16} \\ & M^2_{22} & M^2_{23} & M^2_{24} & M^2_{25} & M^2_{26} \\ & & M^2_{33} & M^2_{34} & M^2_{35} & M^2_{36} \\ & & & M^2_{44} & M^2_{45} & M^2_{46} \\ & & & & M^2_{55} & M^2_{56} \\ & & & & & M^2_{66} \end{pmatrix}, \tag{18}$$

where, in the basis of $\{h_d, h_u, S, S_1, S_2, S_3\}$,

$$\begin{aligned}
M^2_{11} &= \tfrac{(g_1^2+g_2^2)v_d^2}{4} + g_1'^2 Q'^2_{H_d} v_d^2 + \tfrac{A_\lambda \lambda v_S v_u}{\sqrt{2} v_d}, \\
M^2_{12} &= -\tfrac{A_\lambda \lambda v_S}{\sqrt{2}} - \tfrac{(g_1^2+g_2^2) v_d v_u}{4} + (\lambda^2 + g_1'^2 Q'_{H_d} Q'_{H_u}) v_d v_u, \\
M^2_{13} &= \lambda^2 v_d v_s + g_1'^2 Q'_{H_d} Q'_S v_d v_S - \tfrac{A_\lambda \lambda v_u}{\sqrt{2}}, \\
M^2_{1i+3} &= g_1'^2 Q'_{H_d} Q'_{S_i} v_d v_{S_i}, \qquad i = 1,2,3 \\
M^2_{22} &= \tfrac{A_\lambda \lambda v_d v_S}{\sqrt{2} v_u} + \tfrac{1}{4}(g_1^2 + g_2^2 + 4 g_1'^2 Q'_{H_u}) v_u^2, \\
M^2_{23} &= -\tfrac{A_\lambda \lambda v_d}{\sqrt{2}} + (\lambda^2 + g_1'^2 Q'_{H_u} Q'_S) v_u v_S, \\
M^2_{2i+3} &= g_1'^2 Q'_{H_u} Q'_{S_i} v_u v_{S_i}, \qquad i = 1,2,3 \\
M^2_{33} &= \tfrac{1}{2 v_S}(2 g_1'^2 Q'^2_S v_s^3 - 2 m^2_{SS_1} v_{S_1} - 2 m^2_{SS_2} v_{S_2} + \sqrt{2} A_\lambda \lambda v_d v_u), \\
M^2_{3i+3} &= m^2_{SS_i} + g_1'^2 Q'_S Q'_{S_i} v_S v_{S_i} \qquad i = 1,2,3 \quad \text{and} \quad m_{SS_3} = 0 \\
M^2_{44} &= \tfrac{1}{2 v_{S_1}}(2 g_1'^2 Q'^2_{S_1} v^3_{S_1} - 2 m^2_{SS_1} v_S + \sqrt{2} A_\kappa \kappa v_{S_2} v_{S_3}), \\
M^2_{45} &= \tfrac{1}{9}\kappa^2 v_{S_1} v_{S_2} + g_1'^2 Q'_{S_1} Q'_{S_2} v_{S_1} v_{S_2} - \tfrac{A_\kappa \kappa v_{S_3}}{\sqrt{2}}, \\
M^2_{46} &= \tfrac{1}{9}(\kappa^2 + 9 g_1'^2 Q'_{S_1} Q'_{S_3}) v_{S_1} v_{S_3} - \tfrac{A_\kappa \kappa v_{S_2}}{\sqrt{2}}, \\
M^2_{55} &= \tfrac{1}{2 v_{S_2}}(2 g_1'^2 Q'^2_{S_2} v^3_{S_2} - 2 m^2_{SS_2} v_S + \sqrt{2} A_\kappa \kappa v_{S_1} v_{S_3}), \\
M^2_{56} &= \tfrac{1}{9}(\kappa^2 + 9 g_1'^2 Q'_{S_2} Q'_{S_3}) v_{S_2} v_{S_3} - \tfrac{A_\kappa \kappa v_{S_1}}{\sqrt{2}}, \\
M^2_{66} &= g_1'^2 Q'^2_{S_3} v^2_{S_3} + \tfrac{A_\kappa \kappa v_{S_1} v_{S_2}}{\sqrt{2} v_{S_3}}.
\end{aligned}$$

Diagonalizing the mass-square matrix $\mathcal{M}^2_{\text{even}}$ yields six mass eigenstates for the CP-even Higgs bosons in the spectrum. Similarly for the CP-odd Higgs fields,

$$\mathcal{M}^2_{\text{odd}} = \begin{pmatrix} P^2_{11} & P^2_{12} & P^2_{13} & P^2_{14} & P^2_{15} & P^2_{16} \\ & P^2_{22} & P^2_{23} & P^2_{24} & P^2_{25} & P^2_{26} \\ & & P^2_{33} & P^2_{34} & P^2_{35} & P^2_{36} \\ & & & P^2_{44} & P^2_{45} & P^2_{46} \\ & & & & P^2_{55} & P^2_{56} \\ & & & & & P^2_{66} \end{pmatrix}, \tag{19}$$

and, the nonzero elements of $\mathcal{M}^2_{\text{odd}}$ are

$$\begin{aligned}
P^2_{11} &= \frac{A_\lambda \lambda v_S v_u}{\sqrt{2} v_d}, \qquad P^2_{12} = \frac{A_\lambda \lambda v_S}{\sqrt{2}}, \qquad P^2_{13} = \frac{A_\lambda \lambda v_u}{\sqrt{2}}, \\
P^2_{22} &= \frac{A_\lambda \lambda v_d v_S}{\sqrt{2} v_u}, \qquad P^2_{23} \frac{A_\lambda \lambda v_d}{\sqrt{2}}, \\
P^2_{33} &= \frac{1}{2 v_S}(-2 m^2_{SS_1} v_{S_1} - 2 m^2_{SS_2} v_{S_2} + \sqrt{2} A_\lambda \lambda v_d v_u), \qquad P^2_{34} = -m^2_{SS_1}, \qquad P^2_{35} = -m^2_{SS_2}, \\
P^2_{44} &= \frac{1}{2 v_{S_1}}(-2 m^2_{SS_1} v_S + \sqrt{2} A_\kappa \kappa v_{S_2} v_{S_3}), \qquad p^2_{45} = \frac{A_\kappa \kappa v_{S_3}}{\sqrt{2}}, \qquad P^2_{46} = \frac{A_\kappa \kappa v_{S_2}}{\sqrt{2}}, \\
P^2_{55} &= \frac{1}{2 v_{S_2}}(-2 m^2_{SS_2} v_S + \sqrt{2} A_\kappa \kappa v_{S_1} v_{S_3}), \qquad P^2_{56} = \frac{A_\kappa \kappa v_{S_1}}{\sqrt{2}}, \qquad P^2_{66} = \frac{A_\kappa \kappa v_{S_1} v_{S_2}}{\sqrt{2} v_{S_3}}.
\end{aligned}$$

When the mass-square matrix of the CP-odd Higgs fields are diagonalized, two eigenstates out of six happen to be the massless Goldstone bosons, and thus there remain four CP-odd Higgs bosons in the mass spectrum.

As can be seen from the mass-square matrices above, the MSSM Higgs fields and the MSSM singlet scalars of the secluded $U(1)'$ model nontrivially mix in forming the physical Higgs boson states. Such a mixing can yield non-SM Higgs bosons of light mass, which can potentially lead signals in the collider experiments [64]. In this context, profiling the Higgs bosons in the spectrum is of importance in constraining the allowed parameter space of the model. If a Higgs boson mass state, except the SM-like state, is formed mostly by the MSSM Higgs fields, then the current constraints from rare B-meson decays such as $B_s \to \mu^+\mu^-$ and $B \to X_s\gamma$ bound their masses at about 400–500 GeV [78–80]. Thus, if the spectrum involves Higgs bosons lighter than the SM-like Higgs boson are excluded by these constraints if they are significantly formed by the MSSM Higgs fields.

Even though the constrained mentioned above can distinguish the MSSM Higgs fields from the MSSM singlet scalars, they can still interfere through their nontrivial mixing with the MSSM Higgs fields. First, such mixing can allow some decay modes of the light Higgs bosons into the SM particles, which potentially yield a signal at low mass scales. Besides, since the mixing induce a tree-level coupling with the SM-like Higgs boson, the light Higgs boson states can enhance the invisible decays of the SM-like Higgs bosons. One can avoid such inconsistencies by constraining the decay modes of these light Higgs bosons into the SM particles, and the invisible Higgs decays as $\mathrm{BR}(h \to \text{invisible}) \lesssim 10\%$ [88–93].

III. SCANNING PROCEDURE AND EXPERIMENTAL CONSTRAINTS

We employed the SPHENO4.0.4 package [94–96] generated with SARAH 4.14.3 [96–98]. In this package, the weak-scale values of the gauge and Yukawa couplings are evolved to the unification scale M_{GUT} via the renormalization group equations. M_{GUT} is determined by the requirement of the gauge coupling unification, described as $g_3 \approx g_2 = g_1 = g_1'$, where g_3, g_2, and g_1 are the MSSM gauge couplings for $SU(3)_C$, $SU(2)_L$, and $U(1)_Y$ respectively, while g_1' corresponds to the gauge coupling for $U(1)'$. Concerning the contributions from the threshold corrections to the gauge couplings at M_{GUT} arising from some unknown breaking mechanisms of the GUT gauge group, g_3 receives the largest contributions [99], and it is allowed to deviate from the unification point up to about 3%. If a solution does not satisfy this condition within this allowance, SPHENO does not generate an output for such solutions by default. Hence, the existence of an output file guarantees that the solutions are compatible with the unification condition, and g_3 deviates no more than 3%.

TABLE II. Scanned parameter space.

Parameter	Scanned range	Parameter	Scanned range
m_0	[0, 10] TeV	v_S	[1, 20] TeV
$M_{1/2}$	[0, 10] TeV	v_{S_1}	[3, 20] TeV
$\tan\beta$	[1, 50]	v_{S_2}	[3, 20] TeV
$A_0/m0$	$[-3, 3]$	v_{S_3}	[3, 20] TeV
λ	[0.01, 0.5]	A_λ	[0, 10] TeV
κ	[0.1, 1.5]	A_κ	$[-10, 0]$
h_ν	$[10^{-11}, 10^{-7}]$	...	...

After M_{GUT} is calculated, all the SSB parameters, determined with the boundary conditions at M_{GUT}, along with the gauge and Yukawa couplings are evolved back to the weak scale.

We performed random scans over the parameter space, shown in Table II, with the universal boundary conditions. Here m_0 denotes the spontaneous symmetry breaking mass term for all the scalars, while $M_{1/2}$ stands for the SSB mass terms for the gauginos including the one associated with the $\mathrm{U}(1)'$ gauge group. $\tan\beta$ is the ratio of VEVs of the MSSM Higgs doublets, and A_0 is the SSB trilinear scalar interacting term, λ is the coupling associated with the interaction of $\hat{H}_u$, $\hat{H}_d$, and $\hat{S}$ fields while κ is the coupling of the interaction of $\hat{S}_1$, $\hat{S}_2$ and $\hat{S}_3$ fields. Trilinear couplings for λ and κ are defined as λA_λ and κA_κ, respectively at the GUT scale. h_ν is the Yukawa coupling of the term $\hat{L}\hat{H}_u\hat{N}$.

In analyzing the data and implications of the model, we impose the LEP2 bounds on the charged particles such that the model does not yield any new charged particles whose mass is lighter than about 100 GeV [100]. In addition, since it has been significantly being updated, we require that the consistent solutions yield gluino mass as $m_{\tilde{g}} \geq 2100$ GeV. Another important mass bound comes from the Higgs boson. We require one of the Higgs bosons in solutions to exhibit the SM-like Higgs boson properties in terms of its mass and decay channels reported by the ATLAS [101–104] and CMS [105–108] Collaborations. Including the scalars, whose VEVs break the $U(1)'$ symmetry, the low scale spectrum involves six CP-even Higgs boson mass. Since the mixing between the $U(1)'$ breaking scalar fields and the MSSM Higgs fields is expected to be small, the SM-like Higgs boson should be formed mostly by the MSSM Higgs fields. In this context, the SM-like Higgs boson needs be identified not only with its mass, but also its mixing. If a solution yields one of the Higgs bosons $(h_i, i = 1, \ldots 6)$ with a mass of about 125 GeV [109], we also require $|ZH(i,1)|^2 + |ZH(i,2)|^2 \gtrsim 80\%$, where Z_H matrix quantifies the mixing among the Higgs bosons.

Another one of the important constraints arises from the REWSB conditions [110–114] which requires the μ term consistent with EWSB. We also implement the constraints from rare B-meson decays such as $\mathrm{BR}(B \to X_s\gamma)$ [115], $\mathrm{BR}(B_s \to \mu^+\mu^-)$ [116], and $\mathrm{BR}(B_u \to \tau\nu_\tau)$ [117].

TABLE III. The experimental constraints employed in our analyses.

Observable	Constraint	Reference
m_h	[122–128] GeV	[101,120]
$M_{Z'}$	≥4 TeV	[68–73]
$m_{\tilde{g}}$	≥2.1 TeV	[121]
$m_{\tilde{\chi}_1^\pm}, m_{\tilde{\tau}}$	≥100 GeV	[100]
$\mathrm{BR}(B \to X_s\gamma)$	$[2.99\text{–}3.87] \times 10^{-4}(2\sigma)$	[115]
$\mathrm{BR}(B_s \to \mu^+\mu^-)$	$[0.8\text{–}6.2] \times 10^{-9}(2\sigma)$	[116]
$\frac{\mathrm{BR}(B_u \to \tau\nu_\tau)_{\mathrm{Secluded}U(1)'}}{\mathrm{BR}(B_u \to \tau\nu_\tau)_{\mathrm{SM}}}$	$[0.15\text{–}2.41](2\sigma)$	[117]
$\Omega_{\mathrm{CDM}}h^2$	$[0.114\text{–}0.126](5\sigma)$	[118]

Then, we require that the predicted relic density of the neutralino LSP agrees within 5σ with the recent Planck results [118]. The relic density of the LSP and scattering cross sections for direct detection experiments are calculated with MICROMEGAS (version 5.0.9) [119]. The experimental constraints are summarized in Table III. The following list summarizes the relation between colors and constraints imposed in our forthcoming plots.

(a) Gray: Represents the points compatible with the radiative EWSB and neutralino LSP,
(b) Blue: Forms a subset of gray and represents points satisfying the constraints on the SUSY particle masses, Higgs boson mass and its couplings, and B-physics constraints,
(c) Red: Forms a subset of blue and represents the points which are consistent with the Planck bounds on the relic density of LSP neutralino within 5σ together with other constraints mentioned for blue points.

IV. RESULTS

In this section we present our results in light of the constraints discussed in the previous section. First, we focus on the $\mathrm{U}(1)'$ charges which characterizes the secluded $\mathrm{U}(1)'$ model. Figure 1 depicts the $\mathrm{U}(1)'$ charge sets satisfying various theoretical and experimental bounds. The color convention is as listed at the end of Sec. III.

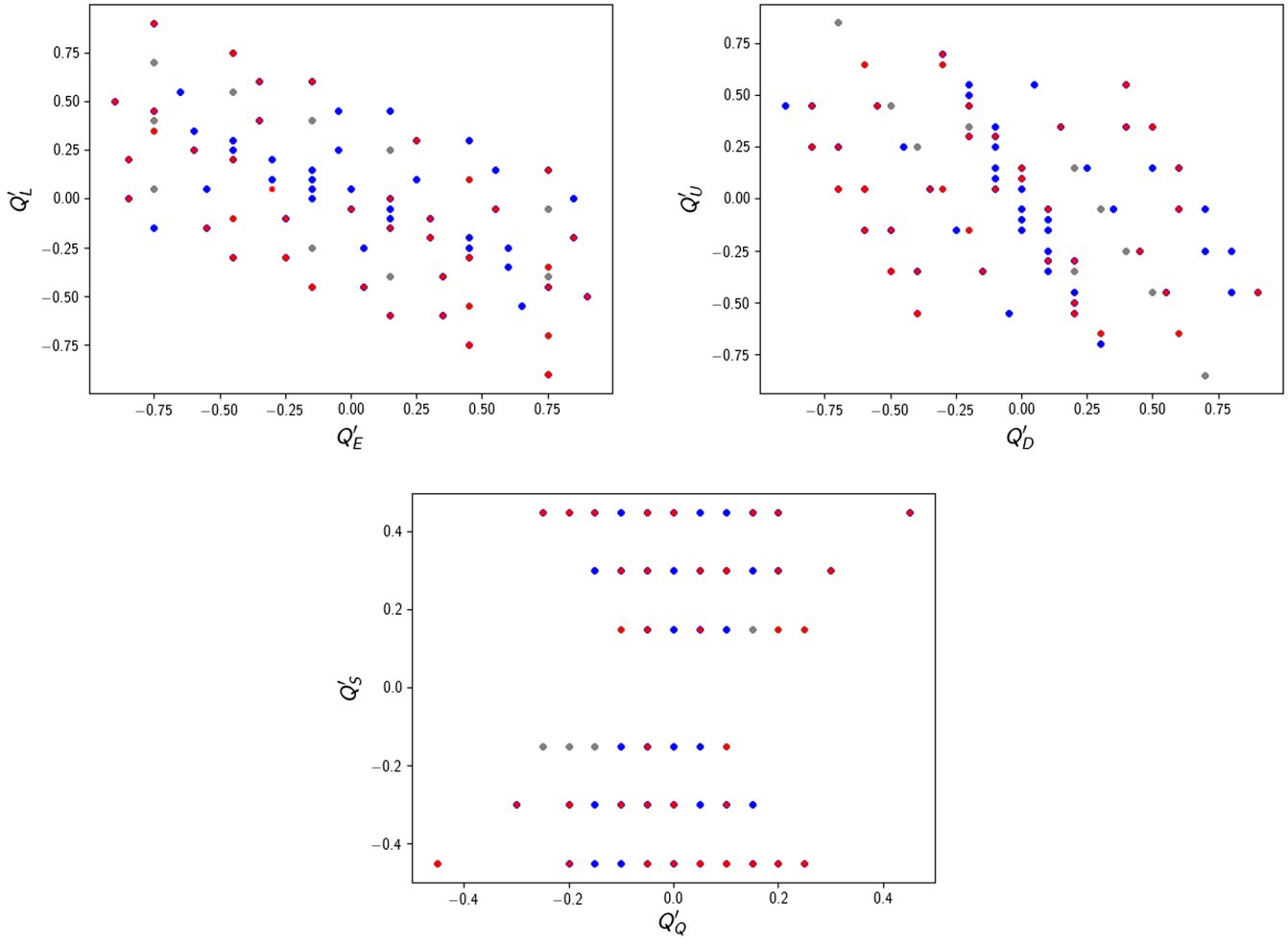

FIG. 1. The distributions of the $\mathrm{U}(1)'$ charges in secluded $\mathrm{U}(1)'$ model allowed by various theoretical and experimental conditions from Sec. III over the following planes: $Q'_L - Q'_E$, $Q'_U - Q'_D$ and $Q'_S - Q'_Q$. The color convention is as listed at the end of Sec. III.

Herein, we show charges for left and right chiral fermions and MSSM singlet by visualising our scan points over the planes $Q'_L - Q'_E$ and $Q'_U - Q'_D$ (top panels), and $Q'_S - Q'_Q$ (bottom panel). Note that the charges are normalized to unity. As can be seen from the top left panel, the constraints allow a large number of different solution sets, and a wide range for the charges can be accommodated, e.g., the $Q'_L, Q'_E \lesssim |0.9|$. As for quarks, the right-handed up-type quark charges (Q'_U) and the right-handed down-type ones (Q'_D) exhibit almost the same behavior (as shown in the top-right panel of the figure). Furthermore, it can easily be read, from the bottom panel, that Q'_S charge is always far away from zero since $Q'_S = -(Q'_{H_u} + Q'_{H_d})$. After applying all theoretical conditions and experimental constraints, Q'_S an Q'_Q charges are restricted to certain regions, $Q'_S, Q'_Q \lesssim |0.5|$. Since there is not a direct anomaly cancellation condition between Q'_Q and Q'_S, it is possible to find various Q'_Q values for the fixed values of Q'_S.

Figure 2 displays the mass spectrum of SUSY particles in $m_{\tilde{t}} - m_{\tilde{b}}$ (left) and $m_{\tilde{\tau}} - m_{\tilde{\nu}}$ (right) planes. The color convention is as listed at the end of Sec. III. The left panel shows that sbottom and stop masses are heavy in general and should be 3 TeV $\lesssim m_{\tilde{b}}$, $m_{\tilde{t}} \lesssim 15$ TeV. Even though these mass scales are far beyond the reach of the current LHC experiments, they can be probed in the future collider searches [122,123]. Similarly, the right panel also reveals that stau can be as light as only 2 TeV, compatible with all experimental bounds. Even though the sneutrino mass can be realized as low as about 500 GeV, it is, in general, heavier than stau for most of the solutions compatible with all experimental bounds.

Figure 3 shows the neutralino and chargino mass spectrum with diagonal lines emphasizing the coannihilation and annihilation channels of LSP neutralino in $m_{\tilde{\chi}_1^\pm} - m_{\tilde{\chi}_1^0}$ (top left), $m_H - m_{\tilde{\chi}_1^0}$ (top right), $m_{A_1} - m_{\tilde{\chi}_1^0}$ (bottom left), and $m_{A_2} - m_{\tilde{\chi}_1^0}$ (bottom right) planes. The color coding is the same as in Fig. 2. As is shown in the $m_{\tilde{\chi}_1^\pm} - m_{\tilde{\chi}_1^0}$ plane, the chargino and neutralino can be as light as about 50–100 GeV. Even though the LSP neutralino mass can be realized, in principle, lighter than 50 GeV, the mass scales below 50 GeV trigger the invisible decays of the SM-like Higgs boson; thus, we consider the solutions with $m_{\tilde{\chi}_1^0} \lesssim 50$ GeV to be excluded. Similarly, the chargino masses lower than 103.5 GeV are excluded as required by the LEP results. Apart from the lower bounds, the LSP neutralino happens mostly to be lighter than about 1 TeV. As discussed before, the MSSM neutralinos cannot be consistent if their masses are lighter than about 500 GeV due to the severe constraints from rare B-meson decays and their relic density. Thus the solutions with $m_{\tilde{\chi}_1^0} \lesssim 500$ GeV should lead to LSPs which are formed mostly by the MSSM singlet fields. The chargino can be as heavy as about 1.5 TeV in the consistent spectra, while its mass can also be at the order of $\mathcal{O}(100)$ GeV. The light chargino solutions are expected to be formed mostly by Higgsinos because of a sub-TeV scale μ term. In this case, if the LSP is formed by singlinos, while the lightest chargino is mostly a Higgsino, then one can identify the chargino-neutralino coannihilation scenario, through the interactions among the MSSM Higgsinos and $U(1)'$ singlinos, in the approximate mass-degeneracy region represented with the diagonal line in the $m_{\tilde{\chi}_1^\pm} - m_{\tilde{\chi}_1^0}$ plane. In this region, the LSP neutralinos coannihilate together with the lightest charginos which leads to lower the relic density of the LSP. Since the solutions compatible with the Planck bound are mostly accumulated around the diagonal line, the chargino-neutralino coannihilation scenario is required by the consistent DM solutions when $m_{\tilde{\chi}_1^\pm} \simeq m_{\tilde{\chi}_1^0} \lesssim 0.75$ TeV.

Even though one can realize consistent DM solutions through chargino-neutralino coannihilation scenario, the

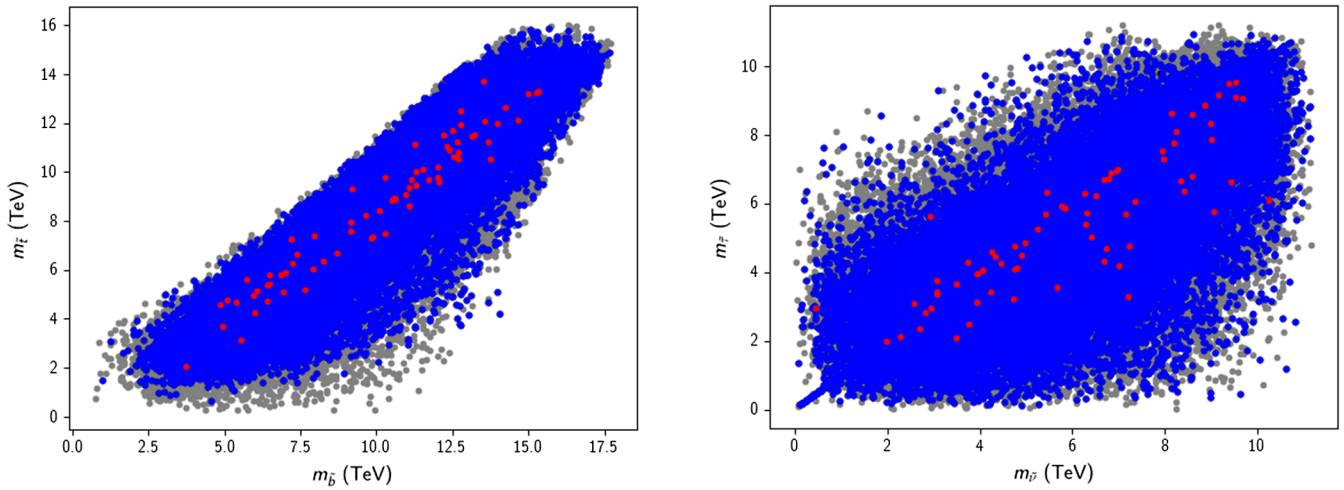

FIG. 2. The mass spectrum of SUSY particles over the following planes: $m_{\tilde{t}} - m_{\tilde{b}}$ (left) and $m_{\tilde{\tau}} - m_{\tilde{\nu}}$ (right). The color convention is as listed at the end of Sec. III.

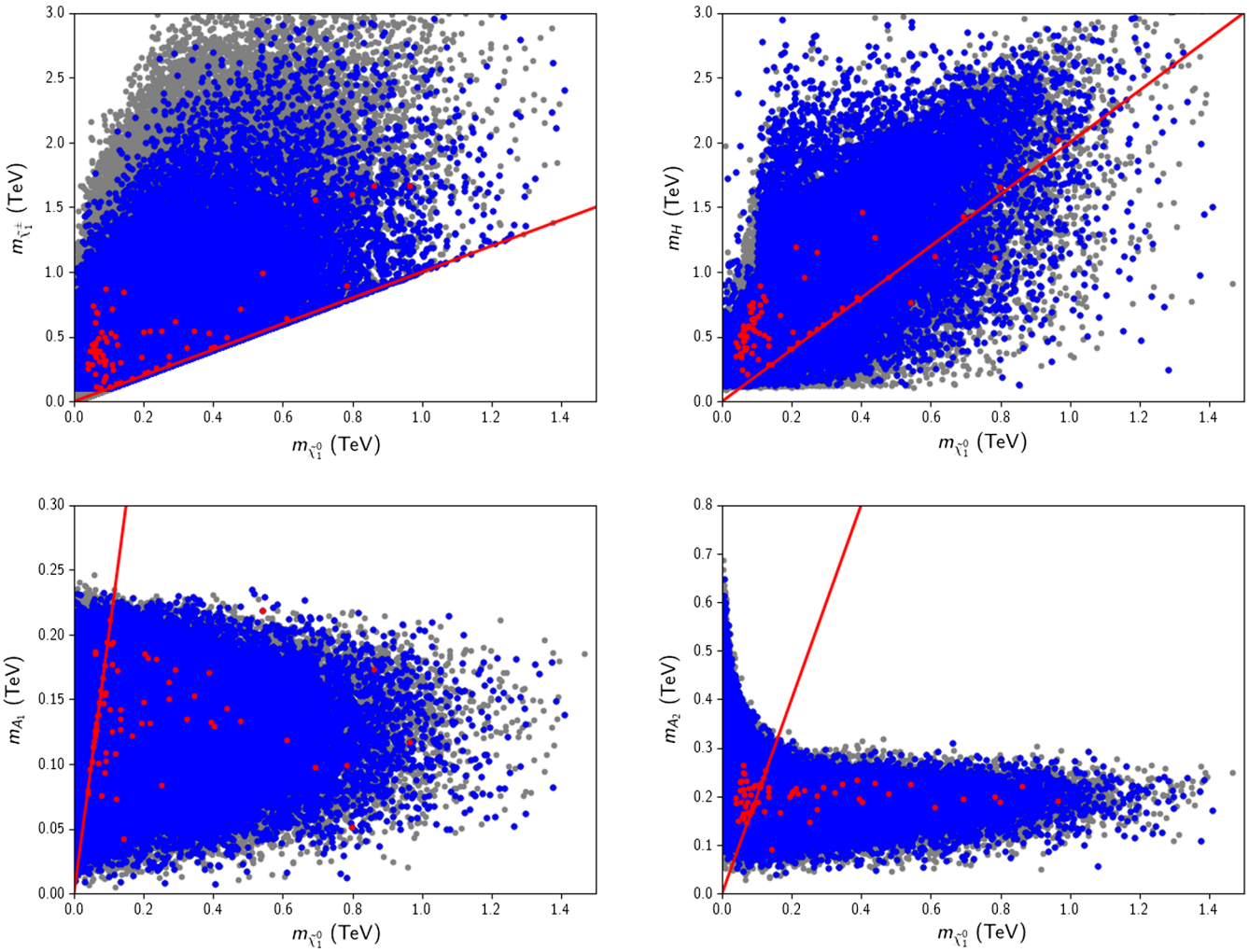

FIG. 3. The mass spectrum of the lightest neutralino and chargino and relic density channels over the following planes; $m_{\tilde{\chi}_1^\pm} - m_{\tilde{\chi}_1^0}$ (top left), $m_H - m_{\tilde{\chi}_1^0}$ (top right), $m_{A_1} - m_{\tilde{\chi}_1^0}$ (bottom left), and $m_{A_2} - m_{\tilde{\chi}_1^0}$ (bottom right). The color convention is as listed at the end of Sec. III.

$m_{\tilde{\chi}_1^\pm} - m_{\tilde{\chi}_1^0}$ plane presents other solutions out of the mass degeneracy region (red points far above the diagonal line). These solutions cannot be identified in the chargino-neutralino coannihilation scenario; thus, the relic density of LSP neutralino should be lowered in other coannihilation and/or annihilation scenarios. Since other SUSY particles are either heavy (as stop, sbottom, and stau shown in Fig. 2) or they do not directly couple to the singlino LSP (as sneutrino), the relic density of LSP neutralino is most likely lowered by its annihilation processes into a neutral Higgs boson as displayed in the $m_H - m_{\tilde{\chi}_1^0}$, $m_{A_1} - m_{\tilde{\chi}_1^0}$, and $m_{A_2} - m_{\tilde{\chi}_1^0}$ planes of Fig. 3. The diagonal lines in these planes indicate the regions where $2m_{\tilde{\chi}_1^0} = m_H, m_{A_1}, m_{A_2}$, respectively. In the regions represented by the diagonal lines, m_H can be as light as about 100 GeV, while it can also be realized as heavy as about 2 TeV. On the other hand, the lighter CP-odd Higgs boson masses are found to be bounded as $m_{A_1} \lesssim 300$ GeV and $m_{A_2} \lesssim 600$ GeV, as shown in the bottom planes of Fig. 3. One can conclude from such results that the LSP neutralino annihilations through the Higgs portal plays an important role to identify consistent DM solutions. Especially the annihilation processes involving CP-odd Higgs bosons significantly lower the relic density of the LSP. Recall that the MSSM Higgs bosons contribute to rare B-meson decays at these mass scales and violate the constraints from B-physics. Thus, these light Higgs bosons should be formed mostly by the MSSM singlet scalars to be consistent with the constraints from rare B-meson decays. Besides, a MSSM singlet Higgs boson can strongly couple to the LSP neutralino and significantly lower its relic density. Even tough these light CP-odd Higgs bosons have MSSM singlet nature, they can interfere in the SM-like Higgs boson decays through $h_1 \to A_i A_i$, if they are formed by the MSSM singlet field S, which is allowed to interact with the MSSM Higgs fields at tree level through the coupling λ. If λ is considerably large, it also enhances the mixing between the MSSM

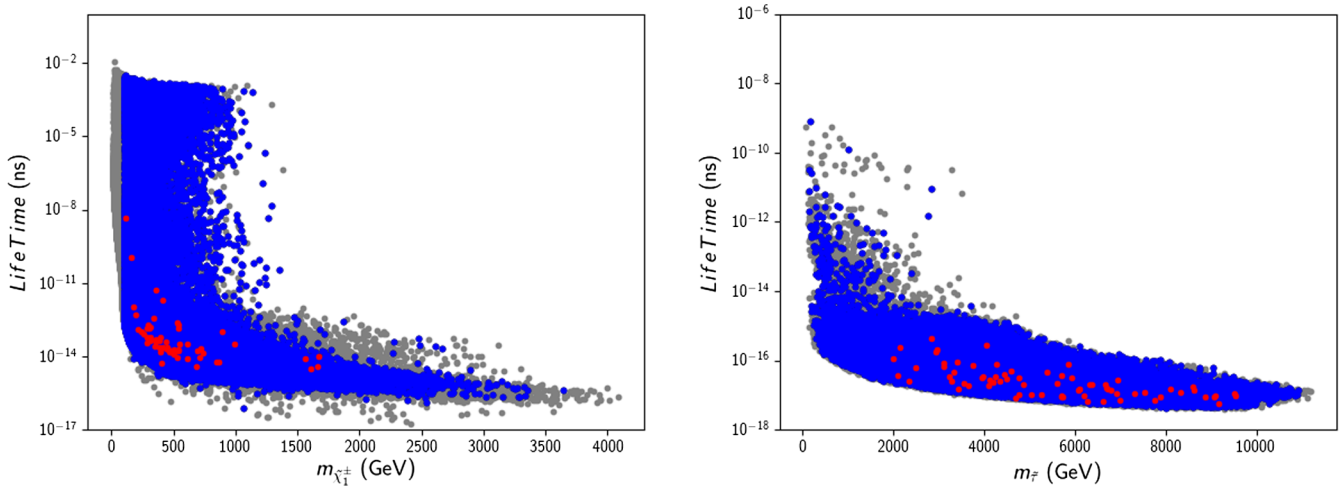

FIG. 4. Lifetime of charged particles such as the chargino (left) and stau (right) in correlation with their masses. The color convention is as listed at the end of Sec. III.

Higgs fields and the MSSM singlet S field. However, such a large mixing receives a strong impact from rare B-meson decays, especially from $B_s \to \mu\mu$. We observed that these light CP-odd Higgs bosons can lead to $\mathrm{BR}(h_1 \to A_1 A_1) \lesssim 15\%$. However, such solutions are excluded by the Planck bound on the relic abundance of LSP neutralino, which favors $\mathrm{BR}(h_1 \to A_1 A_1) \sim 0$. In this context, these light CP-odd Higgs bosons can escape from the current analyses which considers the rare and exotic decays of the SM-like Higgs boson [124–131].

If the spectrum involves charged particles which are nearly degenerate with the LSP neutralino in mass, the current analyses [132,133] yield a strong impact on their lifetime. In the models under phenomenological concern, the stability of such light charged particles can be controlled by the tree-level coupling between NLSP and LSP. Even though the current experimental constraints prevent the strongly-interacting charged particles to be NLSP, the chargino and the sleptons are, in principal, allowed to be NLSP. As discussed before, since the universal SSB gaugino mass terms do not allow the wino to be lighter than bino, the light chargino solutions can be observed only if they are formed by the MSSM Higgsinos, which couple to the MSSM singlet LSP neutralino at tree level. In addition, the universal SSB mass term for the scalar supersymmetric particles lead to stau to be the lightest slepton in the low-scale mass spectrum. However, there is no tree-level coupling between the stau and MSSM singlet LSP neutralino, and the NLSP stau solutions are more likely imply stable staus. Such solutions are strictly excluded by the collider analyses, since they would signal in the collisions as a missing charge. We have plotted the lifetime of these charged particles in Fig. 4 in correlation with their masses. All points are compatible with REWSB and the LSP neutralino condition. The blue points are consistent with the mass bounds and constraints from rare B-meson decays. The red points form a subset of blue and they satisfy the Planck bound on the relic abundance of LSP neutralinos within 5σ. The left panel shows the lifetime of lighter chargino, which is Higgsino-like. All solutions yield chargino lifetime shorter than about 10^{-2} ns and compatible with its current bound [132]. Furthermore, the solutions compatible with the Planck bound on the relic abundance of LSP neutralino (shown in red) can have the charginos, whose lifetime cannot be longer than about 10^{-8} ns. Similarly the right panel display the results for the stau lifetime, which undergoes immediate decay in the solutions within our data, since its life-time is realized to be always shorter than about 10^{-9} ns. This is because the stau is always heavier than some other MSSM particles (such as bino and Higgsinos), which couple to stau at tree level. The DM constraint shorten its lif-time further ($\tau_{\tilde{\tau}} \lesssim 10^{-15}$ ns) as seen from the red points. Note that our plots are insensitive to the mass difference of about 1–2 GeV due to the point size used in plotting. Even though the $m_{\tilde{\chi}_1^\pm} - m_{\tilde{\chi}_1^0}$ in Fig. 3 has some red points on the diagonal line, these solutions still lead to 1–2 GeV mass difference between the chargino and LSP neutralino, and such charginos undergo the $\tilde{\chi}_1^\pm \to q\bar{q}'\tilde{\chi}_1^0$ decay processes after they are being produced at the colliders, where q and q' denote different quarks as required by the electric charge conservation.

In addition to discussions about the coannihilation channels in Fig. 3, each species of neutralinos yield different phenomenology and implications in the dark matter experiments. If the LSP mass eigenstate $\tilde{\chi}_1^0$ is given in terms of interaction eigenstates by the following linear combination using the same basis as the neutralino mass matrix given in Eq. (14).

$$\tilde{\chi}_1^0 = Z_{11}\tilde{B} + Z_{12}\tilde{W}^3 + Z_{13}\tilde{H}_d^0 + Z_{14}\tilde{H}_u^0 + Z_{15}\tilde{S} + Z_{16}\tilde{B}' + Z_{17}\tilde{S}_1 + Z_{18}\tilde{S}_2 + Z_{19}\tilde{S}_3, \tag{20}$$

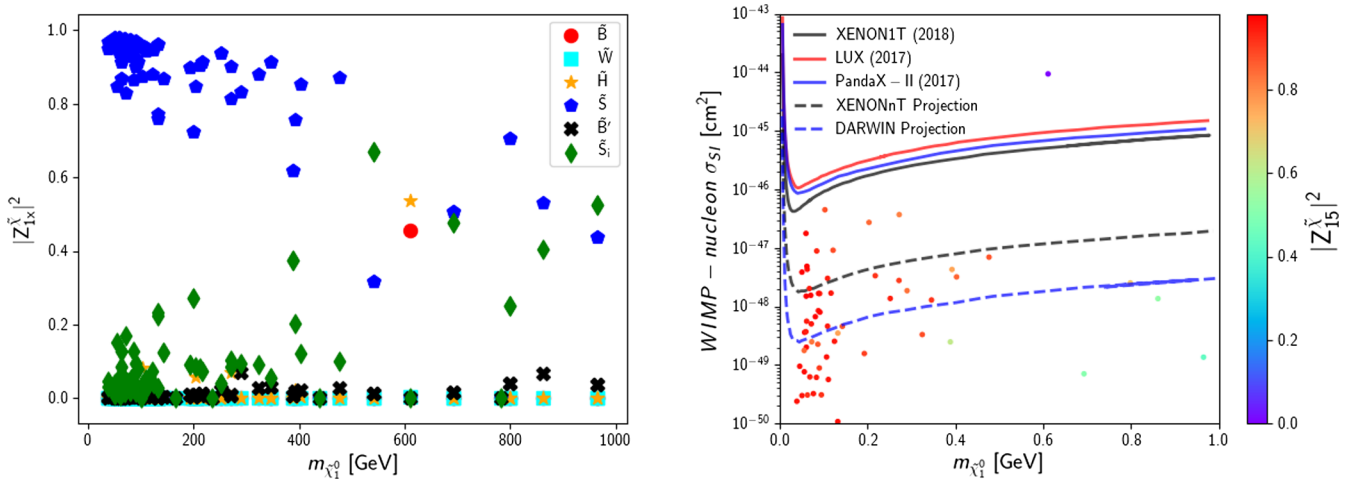

FIG. 5. The composition of the LSP versus its mass (left) and DM-nucleon SI scattering cross section as a function of the mass of the lightest neutralino LSP (right). Limits from current (solid) and future (dashed) experiments are also shown.

where Z_{ij} are elements of the diagonalization matrix encoding the possible mixtures in comprising the neutralino mass eigenstates, $\sum |Z_{ij}|^2 = 1$ by the normalization condition and $|Z_{1j}|^2$ measures the fraction of the jth particle in the composition of LSP neutralino.

The linear superposition of LSP neutralino given in Eq. (20) implies that $U(1)'$ can deviate the LSP neutralino from the MSSM phenomenology by the total fraction of $U(1)'$ particles expressed as $|Z_{15}|^2 + |Z_{16}|^2 + |Z_{17}|^2 + |Z_{18}|^2 + |Z_{19}|^2$. If $|Z_{17}|^2 + |Z_{18}|^2 + |Z_{19}|^2$ dominates the other elements of LSP mass diagonalization matrix, then the dark matter is realized to be mostly decouple from the other particles. In this case, the current sensitivity of the experiments in direct and indirect searches of dark matter cannot probe such solutions. On the other hand, if $|Z_{15}|^2$ is significantly larger, then the dark matter is again composed mostly by the MSSM singlet, i.e., $\tilde{S}$, which interacts with the MSSM particles through the Higgs portal. The current and projected sensitivity of the direct detection of dark matter experiments can provide a potential probe for such solutions. Moreover, even if it does not form the dark matter significantly, it can still alter the dark matter implications through its mixing with the MSSM neutralinos. Finally, even though $\tilde{B}'$ is also theoretically allowed to form the dark matter, the mass is mostly controlled by v_S. Since the heavy mass bound on Z' bounds v_S at about a few TeV from below, the neutralino mass eigenstate, which is mostly formed by $\tilde{B}'$, is found rather to be heavy.

We can summarize the discussion about the LSP neutralino composition and its testable implications in the dark matter experiments with plots given in Fig. 5. In the left panel, we visualize the branching fraction of each neutralino by using different colors and shapes with the mass of the LSP neutralino. The color and shape convention is given in the legend. The points represented in this plane are selected such that they are allowed by all the constraints including the Planck bound on the LSP neutralino relic density. As is seen from the blue pentagons, the light LSP masses ($\lesssim$350 GeV) can be realized when the LSP neutralino is formed mostly by $\tilde{S}$ ($\gtrsim$80%). $\tilde{S}$ still plays a crucial role for relatively large mass scales, since its mixing in the LSP composition is realized at about 40% and more for $m_{\tilde{\chi}^0_1} \gtrsim 400$ GeV. Most of these solutions also reveal that the rest of the LSP neutralino is formed by the other MSSM singlets i.e., $\tilde{S}_1$, $\tilde{S}_2$ and $\tilde{S}_3$. In this context, the dark matter is realized to be almost a MSSM singlet, while it can interact with the MSSM particles through the Higgs portal. As discussed before, the fraction for $\tilde{B}'$ is realized as large as only about 10% and less (black crosses in the left panel of Fig. 5).

The MSSM neutralinos become effective in the LSP composition when $m_{\tilde{\chi}^0_1} \gtrsim 600$ GeV, which can be measured as about 50% bino fraction (red 1), and about 25% for each MSSM Higgsino (turquoise 3 and orange 4). This mass scale bounding the bino-Higgsino mixture is a direct result of the gluino mass bound and the Planck bound on the relic density of LSP neutralino. Since we employ universal gaugino masses at the GUT scale, the gluino mass bound excludes the region where $M_{1/2} \lesssim 600$ GeV. In addition, when the Higgsinos form the LSP neutralino, the relic density constraint is satisfied when $m_{\tilde{\chi}^0_1} \gtrsim 700$ GeV (see, for instance, Refs. [79,134,135]). The Higgsino fraction is also constrained by the results from the direct detection experiments, since it yields large cross sections for the dark matter scattering at nuclei.

As is seen from the discussion above, the secluded $U(1)'$ model yield solutions in which the dark matter is mostly formed by the singlino ($\tilde{S}$). Even though there are not many channels in scattering of dark matter at nuclei, these solutions can be traced down in the direct detection experiments through the Higgs portal, and their signature

TABLE IV. The benchmark points for different scenarios. The points are selected to be consistent with the experimental constraints. All masses are given in TeV, and the cross sections in cm^2.

	Scenario I		Scenario II		Scenario III
Parameters	Point 1	Point 2	Point 3	Point 4	Point 5
g_1'	0.36	0.57	0.41	0.41	0.45
$\tan\beta$	15.7	21.3	12.3	45.7	20.0
$\mu_{\rm eff}$	0.110	0.105	0.389	0.419	0.630
(λ, κ)	(0.02, 0.63)	(0.017, 0.72)	(0.09, 0.67)	(0.09, 1.07)	(0.05, 0.51)
(A_λ, A_κ)	(4.6, −4.2)	(2.2, −3.3)	(3.9, −3.2)	(5.0, −8.6)	(4.8, −3.1)
$(v_{s_1}, v_{s_2}, v_{s_3})$	(15.5, 14.6, 12.6)	(13.0, 8.55, 11.8)	(14.6, 11.2, 14.1)	(11.5, 19.0, 9.65)	(10.0, 10.0, 6.8)
(m_0)	3.835	4.569	9.610	7.267	5.512
$(M_{1/2})$	3.345	9.359	5.500	3.502	1.450
(A_0)	1.305	−2.572	1.154	−3.639	−0.305
$m_{Z'}$	5.53	5.19	6.43	5.69	5.62
$(m_{H_1^0}, m_{H_2^0})$	(0.1243, 0.659)	(0.127, 0.325)	(0.1228, 0.242)	(0.125, 0.783)	(0.1234, 1.121)
$(m_{A_1^0}, m_{A_2^0})$	(0.142, 0.188)	(0.210, 0.223)	(0.117, 0.157)	(0.172, 0.253)	(0.119, 0.179)
$(m_{\tilde{\chi}_1^0}, m_{\tilde{\chi}_2^0})$	(0.103, 0.115)	(0.102, 0.112)	(0.056, 0.408)	(0.124, 0.436)	(0.611, 0.637)
$(m_{\tilde{\chi}_1^\pm}, m_{\tilde{\chi}_2^\pm})$	(0.117, 2.783)	(0.113, 7.813)	(0.409, 4.638)	(0.438, 2.973)	(643, 1.239)
$m_{H^\pm}$	2.872	2.201	4.327	9.796	7.847
$(m_{\tilde{t}_L}, m_{\tilde{c}_L}, m_{\tilde{u}_L})$	(5.37, 6.89, 7.13)	(12.1, 15.4, 16.3)	(9.59, 12.8, 13.7)	(6.61, 9.22, 9.53)	(4.58, 5.92, 6.38)
$(m_{\tilde{t}_R}, m_{\tilde{c}_R}, m_{\tilde{u}_R})$	(6.41, 6.89, 7.13)	(14.6, 15.4, 16.3)	(12.2, 12.8, 13.7)	(7.38, 9.22, 9.53)	(4.89, 5.92, 6.38)
$(m_{\tilde{b}_L}, m_{\tilde{s}_L}, m_{\tilde{d}_L})$	(6.41, 6.82, 7.13)	(14.6, 15.4, 16.3)	(12.0, 12.1, 13.7)	(7.37, 9.39, 9.53)	(4.88, 5.92, 6.51)
$(m_{\tilde{b}_R}, m_{\tilde{s}_R}, m_{\tilde{d}_R})$	(6.75, 6.82, 7.13)	(15.1, 15.4, 16.3)	(12.2, 12.1, 13.7)	(7.52, 9.39, 9.53)	(6.29, 5.92, 6.51)
$(m_{\tilde{\tau}_L}, m_{\tilde{\mu}_L}, m_{\tilde{e}_L})$	(3.96, 4.03, 4.34)	(4.27, 4.58, 7.80)	(8.87, 8.91, 10.2)	(5.03, 7.55, 7.57)	(4.87, 5.16, 6.24)
$(m_{\tilde{\tau}_R}, m_{\tilde{\mu}_R}, m_{\tilde{e}_R})$	(4.31, 4.03, 4.34)	(7.71, 4.58, 7.80)	(10.1, 8.91, 10.2)	(6.41, 7.55, 7.57)	(6.12, 5.16, 6.24)
$(m_{\tilde{\nu}_{\tau_L}}, m_{\tilde{\nu}_{\mu_L}}, m_{\tilde{\nu}_{e_L}})$	(3.97, 3.97, 4.34)	(3.73, 3.73, 7.80)	(8.87, 8.91, 10.9)	(6.41, 7.26, 7.55)	(4.98, 4.98, 6.24)
$(m_{\tilde{\nu}_{\tau_R}}, m_{\tilde{\nu}_{\mu_R}}, m_{\tilde{\nu}_{e_R}})$	(4.30, 3.97, 4.34)	(7.71, 3.73, 7.80)	(10.9, 8.91, 10.9)	(7.26, 7.26, 7.55)	(6.12, 4.98, 6.24)
$\Omega_{\rm DM}h^2$	0.1146	0.1161	0.1253	0.1178	0.1222
$\sigma_{\rm SI}$	4.59×10^{-47}	1.69×10^{-48}	3.65×10^{-49}	2.61×10^{-49}	9.64×10^{-45}

can be significant depending on how strongly it interacts with the MSSM Higgs fields. The right panel of Fig. 5 show the results for the spin-independent scattering cross section of dark matter with respect to its mass. The represented solutions are selected to be consistent with the constraints employed in our analyses. The experimental results from the direct detection experiments are represented with the curves. The black, blue, and red solid lines show XENON1T [136], PandaX-II [137] and LUX [138] upper limits for the SI $\tilde{\chi}_1^0$—nucleon cross section, respectively, while the black and blue dashed lines illustrate the prospects of the XENONnT and DARWIN for future experiments [139], respectively. We also display a color bar which relates the color coding to the Singlino fraction in the composition of LSP. The red points correspond to Singlino-like dark matter in which the singlino fraction is realized greater than about 70%. The solutions with $m_{\tilde{\chi}_1^0} \lesssim$ 350 GeV yielding scattering cross sections larger than about 2×10^{-48} cm^2 can be tested in XENON experiment soon, while those with $\sigma_{\rm SI} \in [3 \times 10^{49} - 2 \times 10^{48}]$ cm^2 are expected to be probed by the DARWIN collaboration. DARWIN will also be able to test the singlino dark matter when the LSP mass is relatively heavier (∼500 GeV). Finally, we also display a solution exemplifying the MSSM-like dark matter (blue). These solutions were identified as Bino-Higgsino mixture in the previous discussion, and as is seen from the right plane, the direct detection experiments yield a strong negative impact on such solutions, since it predicts a large scattering cross section.

Before concluding, we present six benchmark points in Table IV to exemplify our findings. The results discussed above can be classified into three scenarios as grouped in Table IV. Scenarios I and II involve the solutions of MSSM singlet LSP, and the MSSM-like LSP solutions refer to Scenario III. Scenario I and Scenario II differ from each other in chargino mass. The mass spectra in Scenario I includes charginos nearly mass degenerate with the LSP neutralino, while it is much heavier than the LSP neutralino in Scenario II. The first two points in Table IV exemplify the solutions in Scenario I. The correct relic density of LSP neutralino for these solutions is satisfied through the chargino-neutralino coannihilation scenario. Point 1 predicts $\sigma_{\rm SI} \simeq 5 \times 10^{-46}$ cm^2 for the spin-independent scattering of DM, which can be tested soon in XENON

TABLE V. Sets of $U(1)'$ charges for the benchmark points listed in Table IV. The charges satisfy the conditions of gauge invariance (Eq. (3) in the secluded $U(1)'$ model described by the superpotential (Eq. (2) and of anomaly cancellation (Eqs. (4)–(9)).

	Scenario I		Scenario II		Scenario III
Parameters	Point 1	Point 2	Point 3	Point 4	Point 5
Q'_Q	0.0	−0.05	−0.2	0.2	−0.15
Q'_U	−0.45	−0.3	0.35	−0.35	0.35
Q'_D	0.9	0.1	0.5	−0.5	0.4
Q'_L	0.15	0.05	0.75	−0.75	0.6
Q'_N	−0.6	−0.4	−0.6	0.6	−0.4
Q'_E	0.75	−0.3	−0.45	0.45	−0.35
Q'_{H_u}	0.45	0.35	−0.15	0.15	−0.20
Q'_{H_d}	−0.9	−0.05	−0.3	0.3	−0.25
Q'_S	0.45	−0.3	0.45	−0.45	0.45
Q'_{S_1}	0.45	−0.3	0.45	−0.45	0.45
Q'_{S_2}	0.45	−0.3	0.45	−0.45	0.45
Q'_{S_3}	−0.9	0.6	−0.9	0.9	−0.9

experiments. Point 2 displays a solution for A-resonance. Points 3 and 4 represent the solutions in Scenario II in which the relic density constraint is satisfied only through A resonance. Point 3 yields $\sigma_{\rm SI} \simeq 10^{-48}$ cm^2, and Darwin experiments will be able to test such solutions in near future. Point 4 depicts a solution in which two LSP neutralinos annihilate into the second CP-odd Higgs boson of mass about 250 GeV. Finally Point 5 displays solutions for Scenario III in which the LSP neutralino is formed by the MSSM neutralinos, which is mostly Higgsino in our model. Such solutions lead to very large cross sections in DM scattering with nuclei ($\sim 10^{-44}$ cm^2) and they are excluded by the current constraints set by the direct detection experiments. We also list the sets of $U(1)'$ charges for these benchmark points in Table V. The solutions in Scenario I favor sets of charges in which the left-handed quark and lepton fields have relatively low charges under the $U(1)'$ group. Scenario II depicts a certain magnitudes of the $U(1)'$ charges, while their sign could be negative or positive. Scenario III reveals a fact that all the fields are considerably charged under $U(1)'$ group if the LSP neutralino is formed by the MSSM neutralinos.

V. CONCLUSION

We realized that the $U(1)'$ extension, which extends the MSSM with MSSM singlet particles considerably alter the DM phenomenology for the LSP neutralino masses from about 100 GeV to 1 TeV. This mass scale can be divided into three scenarios, which follow different manifestations in the results of the relic abundance of LSP neutralino and its scattering with nuclei. The typical mass spectrum in all scenarios involves two light CP-odd Higgs bosons whose masses are lighter than about 200 GeV and 600 GeV, respectively. Due to the strong impact from rare B meson decays employed in our analyses, the MSSM Higgs bosons cannot be lighter than about 500 GeV, and such light Higgs boson solutions can be consistent with the constraints from rare B-meson decays only when they are formed mostly by the MSSM singlet fields. These CP-odd Higgs bosons play important roles to reduce the relic abundance of LSP neutralino compatible with the current Planck bounds.

Scenario I involves the LSP neutralino as light as about 100 GeV together with light charginos. It can be seen easily that the LSP composition involves more than about 80% singlino, while the remaining $\lesssim$20% also formed by the other MSSM singlet fields, $S_{1,2,3}$. This composition holds in almost all the solutions with $m_{\tilde{\chi}_1^0} \lesssim 500$ GeV. Thus, the secluded $U(1)'$ model yields mostly MSSM singlet DM which can considerably interact with the MSSM particles through the Higgs portal. Singlino still takes part in the DM phenomenology for heavier LSP neutralino solutions, since its percentage in the LSP composition is realized greater than about 50% for $m_{\tilde{\chi}_1^0} \lesssim 1$ TeV. In this region, the MSSM Higgsinos are involved in the LSP decomposition up to about 40%. The correct relic density for the LSP neutralino is partly satisfied through the chargino-neutralino coannihilation scenario in Scenario I up to about $m_{\tilde{\chi}_1^\pm} \lesssim 750$ GeV. The latest LHC constraints, especially the gluino mass bound, result in binos and winos heavier than about 300 GeV at the low-scale SUSY spectrum, and hence the lighter chargino state is formed mostly by MSSM Higgsinos, so the chargino couples to the MSSM singlet LSP neutralino at tree-level. We realized that this coupling lead to a life-time for such light charginos always shorter than about 10^{-2} ns. We observed that the chargino life-time lasts longer if the Wino takes part in decomposition of the lighter chargino, but the solutions with $\tau_{\tilde{\chi}_1^\pm} \gtrsim 10^{-8}$ ns are excluded by the current Planck bound on the relic abundance of LSP neutralino. The solutions in Scenario II can also be characterized by the singlino LSP neutralino in the similar mass range, but these solutions involve relatively heavier charginos, and the chargino-neutralino coannihilation scenario is not realized in this Scenario. The correct relic density of the LSP neutralino is satisfied through its annihilation into the lighter CP-odd Higgs bosons, which are mostly formed by the MSSM singlet Higgs bosons in our model.

One may expect small scattering cross section for the LSP neutralino due to its dominant singlet nature under the MSSM gauge group. However, as mentioned above, the singlino is allowed to interact with the MSSM particles through the Higgs portal, which can potentially enhance its scattering cross section. We observed that the singlino LSP solutions can predict DM spin-independent cross section in the range $\sim 4 \times 10^{46}$ cm^2–10^{-50} cm^2 for the singlinolike LSP. These solutions are expected to be tested in XENONnT experiments up to about $\sigma_{\rm SI} \sim 2 \times 10^{-48}$ cm^2, while Darwin can lower the testable cross section scale to about 3×10^{-49} cm^2 in near future.

We identify another class of solutions which can be classified as Scenario III. In this scenario, the LSP neutralino can still exhibit MSSM singlet nature, but the MSSM neutralinos considerably takes part in its decomposition since their mixing with the singlino can be more than about 50%. Furthermore, this scenario can also yield MSSM-like LSP neutralino, which is mostly formed by the MSSM Higgsinos. The CMSSM-like gaugino mass relation yield $M_2 > \mu$ and results in Higgsino-like lighter chargino states. Such solutions typically yield nearly mass degenerate chargino and LSP neutralino and they fall into the chargino-neutralino coannihilation region. The light CP-odd Higgs bosons do not take significant part in satisfying the correct relic density in this region. Even though such solutions can be consistent with the experimental constraints employed in our analyses, they receive a strong negative impact from the direct detection DM experiments due to the large scattering cross sections of Higgsino-like LSP neutralino. We find that its scattering cross section is of the order about 10^{-44} cm^2, which is severely excluded by the current results from the direct detection experiments.

ACKNOWLEDGMENTS

The work of Y. H. is supported by The Scientific and Technological Research Council of Turkey (TUBITAK) in the framework of the 2219-International Postdoctoral Research Fellowship Programme, and by Balikesir University Scientific Research Projects with Grant No. BAP-2017/198. The research of C. S. U. was supported in part by the Spanish MICINN, under Grant No. PID2019–107844 GB-C22. The authors also acknowledge the use of the IRIDIS High Performance Computing Facility, and associated support services at the University of Southampton, in the completion of this work.

[1] E. Gildener, Gauge symmetry hierarchies, Phys. Rev. D **14**, 1667 (1976).
[2] E. Gildener, Gauge symmetry hierarchies revisited, Phys. Lett. **92B**, 111 (1980).
[3] S. Weinberg, Gauge hierarchies, Phys. Lett. **82B**, 387 (1979).
[4] L. Susskind, Dynamics of spontaneous symmetry breaking in the Weinberg-Salam theory, Phys. Rev. D **20**, 2619 (1979).
[5] M. J. G. Veltman, The infrared—ultraviolet connection, Acta Phys. Pol. B **12**, 437 (1981).
[6] G. Degrassi, S. Di Vita, J. Elias-Miro, J. R. Espinosa, G. F. Giudice, G. Isidori, and Alessandro Strumia, Higgs mass and vacuum stability in the Standard Model at NNLO, J. High Energy Phys. 08 (2012) 098.
[7] F. Bezrukov, M. Y. Kalmykov, B. A. Kniehl, and M. Shaposhnikov, Higgs boson mass and new physics, J. High Energy Phys. 10 (2012) 140.
[8] D. Buttazzo, G. Degrassi, P. P. Giardino, G. F. Giudice, F. Sala, A. Salvio, and Alessandro Strumia, Investigating the near-criticality of the Higgs boson, J. High Energy Phys. 12 (2013) 089.
[9] V. Branchina and E. Messina, Stability, Higgs Boson Mass and New Physics, Phys. Rev. Lett. **111**, 241801 (2013).
[10] V. Branchina, E. Messina, and A. Platania, Top mass determination, Higgs inflation, and vacuum stability, J. High Energy Phys. 09 (2014) 182.
[11] A. R. Fazio and E. A. Reyes R., The lightest Higgs boson mass of the MSSM at three-loop accuracy, Nucl. Phys. **B942**, 164 (2019).
[12] A. de Gouvea, S. Gopalakrishna, and W. Porod, Stop decay into right-handed sneutrino LSP at hadron colliders, J. High Energy Phys. 11 (2006) 050.
[13] M. Chala, A. Delgado, G. Nardini, and M. Quiros, A light sneutrino rescues the light stop, J. High Energy Phys. 04 (2017) 097.
[14] C. T. Potter, Natural NMSSM with a light singlet Higgs and singlino LSP, Eur. Phys. J. C **76**, 44 (2016).
[15] L. Delle Rose, S. Khalil, S. J. D. King, S. Kulkarni, C. Marzo, S. Moretti, and Cem S. Un, Sneutrino dark matter in the BLSSM, J. High Energy Phys. 07 (2018) 100.
[16] L. Delle Rose, S. Khalil, S. J. D. King, C. Marzo, S. Moretti, and C. S. Un, Naturalness and dark matter in the supersymmetric $B-L$ extension of the standard model, Phys. Rev. D **96**, 055004 (2017).
[17] W. Ahmed, S. Raza, Q. Shafi, C. S. Un, and B. Zhu, Sparticle spectroscopy and dark matter in a $U(1)_{B-L}$ extension of MSSM, J. High Energy Phys. 01 (2021) 161.
[18] K. J. Bae, H. Baer, V. Barger, and D. Sengupta, Revisiting the SUSY μ problem and its solutions in the LHC era, Phys. Rev. D **99**, 115027 (2019).
[19] M. Cvetic, D. A. Demir, J. R. Espinosa, L. L. Everett, and P. Langacker, Electroweak breaking and the mu problem in supergravity models with an additional U(1), Phys. Rev. D **56**, 2861 (1997).
[20] A. E. Nelson, N. Rius, V. Sanz, and M. Unsal, The minimal supersymmetric model without a mu term, J. High Energy Phys. 08 (2002) 039.
[21] J. R. Ellis, G. K. Leontaris, and J. Rizos, Implications of anomalous U(1) symmetry in unified models: The Flipped $SU(5) \times U(1)$ paradigm, J. High Energy Phys. 05 (2000) 001.
[22] M. Frank, L. Selbuz, L. Solmaz, and I. Turan, Higgs bosons in supersymmetric U(1)' models with CP violation, Phys. Rev. D **87**, 075007 (2013).

[23] S. Bertolini, L. Di Luzio, and M. Malinsky, Minimal flipped $SO(10) \times U(1)$ supersymmetric Higgs model, Phys. Rev. D **83**, 035002 (2011).

[24] P. Athron, S. F. King, D. J. Miller, S. Moretti, and R. Nevzorov, Predictions of the constrained exceptional supersymmetric standard model, Phys. Lett. B **681**, 448 (2009).

[25] M. Frank, L. Selbuz, and I. Turan, Heavy gauge bosons in supersymmetric $U(1)'$ models at present and future hadron colliders, Eur. Phys. J. C **81**, 466 (2021).

[26] D. Suematsu and Y. Yamagishi, Radiative symmetry breaking in a supersymmetric model with an extra U(1), Int. J. Mod. Phys. A **10**, 4521 (1995).

[27] H.-S. Lee, K. T. Matchev, and T. T. Wang, A U(1) -prime solution to the μ^- problem and the proton decay problem in supersymmetry without R-parity, Phys. Rev. D **77**, 015016 (2008).

[28] D. A. Demir, Two Higgs doublet models from TeV scale supersymmetric extra U(1) models, Phys. Rev. D **59**, 015002 (1998).

[29] M. Cvetic and P. Langacker, New gauge bosons from string models, Mod. Phys. Lett. A **11**, 1247 (1996).

[30] J. L. Hewett and T. G. Rizzo, Low-energy phenomenology of superstring inspired E(6) models, Phys. Rep. **183**, 193 (1989).

[31] C. T. Hill and E. H. Simmons, Strong dynamics and electroweak symmetry breaking, Phys. Rep. **381**, 235 (2003).

[32] S. Khalil, TeV-scale gauged B-L symmetry with inverse seesaw mechanism, Phys. Rev. D **82**, 077702 (2010).

[33] Super-Kamiokande Collaboration, Atmospheric neutrino oscillation analysis with sub-leading effects in Super-Kamiokande I, II, and III, Phys. Rev. D **81**, 092004 (2010).

[34] Y. Hicyilmaz, L. Solmaz, S. H. Tanyildizi, and C. S. Un, Least fine-tuned U (1) extended SSM, Nucl. Phys. **B933**, 275 (2018).

[35] N. Okada, S. Okada, D. Raut, and Q. Shafi, Dark matter Z' and XENON1T excess from $U(1)_X$ extended standard model, Phys. Lett. B **810**, 135785 (2020).

[36] N. Nath, N. Okada, S. Okada, D. Raut, and Q. Shafi, Light Z' and Dirac fermion dark matter in the $B-L$ model, arXiv:2112.08960.

[37] M. Lindner, Y. Mambrini, T. B. de Melo, and F. S. Queiroz, XENON1T anomaly: A light Z' from a two Higgs doublet model, Phys. Lett. B **811**, 135972 (2020).

[38] M. Abdullah, M. Dalchenko, T. Kamon, D. Rathjens, and A. Thompson, A heavy neutral gauge boson near the Z boson mass pole via third generation fermions at the LHC, Phys. Lett. B **803**, 135326 (2020).

[39] M. Frank, Evading Z' boson mass limits in $U(1)'$ supersymmetric models, Eur. Phys. J. Special Topics **229**, 3205 (2020).

[40] J. Erler, P. Langacker, and T.-J. Li, The Z-Z' mass hierarchy in a supersymmetric model with a secluded U(1)-prime breaking sector, Phys. Rev. D **66**, 015002 (2002).

[41] C.-W. Chiang and E. Senaha, CP violation in the secluded U(1)-prime-extended MSSM, J. High Energy Phys. 06 (2008) 019.

[42] Y. Hiçyılmaz and S. Moretti, Characterisation of dark matter in direct detection experiments: Singlino versus Higgsino, Nucl. Phys. **B967**, 115404 (2021).

[43] M. Frank, Y. Hiçyılmaz, S. Moretti, and O. Özdal, E_6 motivated UMSSM confronts experimental data, J. High Energy Phys. 05 (2020) 123.

[44] Y. Hiçyılmaz, L. Selbuz, L. Solmaz, and C. S. Ün, Charged Higgs boson in MSSM and beyond, Phys. Rev. D **97**, 115041 (2018).

[45] D. A. Demir, M. Frank, L. Selbuz, and I. Turan, Scalar neutrinos at the LHC, Phys. Rev. D **83**, 095001 (2011).

[46] M. Frank, L. Selbuz, and I. Turan, Neutralino and chargino production in $U(1)'$ at the LHC, Eur. Phys. J. C **73**, 2656 (2013).

[47] A. De Rujula, H. Georgi, and S. L. Glashow, Flavor Goniometry by Proton Decay, Phys. Rev. Lett. **45**, 413 (1980).

[48] J. P. Derendinger, J. E. Kim, and D. V. Nanopoulos, Anti-SU(5), Phys. Lett. **139B**, 170 (1984).

[49] I. Antoniadis, J. R. Ellis, J. S. Hagelin, and D. V. Nanopoulos, Supersymmetric flipped SU(5) revitalized, Phys. Lett. B **194**, 231 (1987).

[50] J. R. Ellis, J. S. Hagelin, S. Kelley, and D. V. Nanopoulos, Aspects of the flipped unification of strong, weak and electromagnetic interactions, Nucl. Phys. **B311**, 1 (1988).

[51] G. Lazarides, C. Panagiotakopoulos, and Q. Shafi, Superstring motivated gauge models based on a rank six subgroup of $E(6)$, Z. Phys. C **34**, 553 (1987).

[52] Q. Shafi, E(6) as a unifying gauge symmetry, Phys. Lett. **79B**, 301 (1978).

[53] F. Gursey, P. Ramond, and P. Sikivie, A universal gauge theory model based on E6, Phys. Lett. **60B**, 177 (1976).

[54] B. Bajc and V. Susič, Towards the minimal renormalizable supersymmetric E_6 model, J. High Energy Phys. 02 (2014) 058.

[55] D. A. Demir, G. L. Kane, and T. T. Wang, The minimal $U(1)'$ extension of the MSSM, Phys. Rev. D **72**, 015012 (2005).

[56] J. Ellis, A. Mustafayev, and K. A. Olive, Constrained supersymmetric flipped SU(5) GUT phenomenology, Eur. Phys. J. C **71**, 1689 (2011).

[57] I. Gogoladze, R. Khalid, S. Raza, and Q. Shafi, CDMS II inspired neutralino dark matter in flipped SU(5), Mod. Phys. Lett. A **25**, 3371 (2010).

[58] L. Delle Rose, S. Khalil, S. J. D. King, S. Moretti, and A. M. Thabt, Atomki anomaly in family-dependent $U(1)'$ extension of the standard model, Phys. Rev. D **99**, 055022 (2019).

[59] J. Erler, P. Langacker, S. Munir, and E. Rojas, Improved constraints on Z-prime bosons from electroweak precision data, J. High Energy Phys. 08 (2009) 017.

[60] F. del Aguila, J. de Blas, and M. Perez-Victoria, Electroweak limits on general new vector bosons, J. High Energy Phys. 09 (2010) 033.

[61] CDF Collaboration, Search for WW and WZ Resonances Decaying to Electron, Missing E_T, and Two Jets in $p\bar{p}$ Collisions at $\sqrt{s} = 1.96$ TeV, Phys. Rev. Lett. **104**, 241801 (2010).

[62] G. Cacciapaglia, C. Csaki, G. Marandella, and A. Strumia, The minimal set of electroweak precision parameters, Phys. Rev. D **74**, 033011 (2006).
[63] B. O'Leary, W. Porod, and F. Staub, Mass spectrum of the minimal SUSY B-L model, J. High Energy Phys. 05 (2012) 042.
[64] C. S. Un and O. Ozdal, Mass spectrum and Higgs profile in BLSSM, Phys. Rev. D **93**, 055024 (2016).
[65] P. Langacker, The physics of heavy Z' gauge bosons, Rev. Mod. Phys. **81**, 1199 (2009).
[66] K. S. Babu, C. F. Kolda, and J. March-Russell, Implications of generalized Z-Z-prime mixing, Phys. Rev. D **57**, 6788 (1998).
[67] P. Langacker and J. Wang, U(1)-prime symmetry breaking in supersymmetric E(6) models, Phys. Rev. D **58**, 115010 (1998).
[68] A. A. Pankov, P. Osland, I. A. Serenkova, and V. A. Bednyakov, High-precision limits on $W - W'$ and $Z - Z'$ mixing from diboson production using the full LHC Run 2 ATLAS data set, Eur. Phys. J. C **80**, 503 (2020).
[69] I. D. Bobovnikov, P. Osland, and A. A. Pankov, Improved constraints on the mixing and mass of Z' bosons from resonant diboson searches at the LHC at $\sqrt{s} = 13$ TeV and predictions for Run II, Phys. Rev. D **98**, 095029 (2018).
[70] CMS Collaboration, Combination of diboson resonance searches at 8 and 13 TeV, Report No. CMS-PAS-B2G-16-007 (2016).
[71] J. Lao, C. Cai, Z.-H. Yu, Y.-P. Zeng, and H.-H. Zhang, Fermionic and scalar dark matter with hidden U(1) gauge interaction and kinetic mixing, Phys. Rev. D **101**, 095031 (2020).
[72] ATLAS Collaboration, Search for high-mass dilepton resonances using 139 fb^{-1} of pp collision data collected at $\sqrt{s} = 13$ TeV with the ATLAS detector, Phys. Lett. B **796**, 68 (2019).
[73] CMS Collaboration, Search for a narrow resonance in high-mass dilepton final states in proton-proton collisions using 140 fb^{-1} of data at $\sqrt{s} = 13$ TeV, Report No. CMS-PAS-EXO-19-019 (2019).
[74] J. Kang and P. Langacker, Z' discovery limits for supersymmetric E(6) models, Phys. Rev. D **71**, 035014 (2005).
[75] G. Lazarides and Q. Shafi, R symmetry in minimal supersymmetry standard model and beyond with several consequences, Phys. Rev. D **58**, 071702 (1998).
[76] ATLAS, CMS Collaborations, Exotic searches by ATLAS and CMS, J. Phys. Conf. Ser. **1690**, 012169 (2020).
[77] ATLAS Collaboration, Search for squarks and gluinos in final states with jets and missing transverse momentum using 36 fb^{-1} of $\sqrt{s} = 13$ TeV pp collision data with the ATLAS detector, Phys. Rev. D **97**, 112001 (2018).
[78] K. S. Babu, I. Gogoladze, and C. S. Un, Proton lifetime in minimal SUSY SU(5) in light of LHC results, J. High Energy Phys. 02 (2022) 164.
[79] S. Raza, Q. Shafi, and C. S. Un, $b - \tau$ Yukawa unification in SUSY SU(5) with mirage mediation: LHC and dark matter implications, J. High Energy Phys. 05 (2019) 046.
[80] M. E. Gómez, Q. Shafi, and C. S. Un, Testing Yukawa unification at LHC Run-3 and HL-LHC, J. High Energy Phys. 07 (2020) 096.
[81] R. Krall and M. Reece, Last electroweak WIMP standing: Pseudo-Dirac higgsino status and compact stars as future probes, Chin. Phys. C **42**, 043105 (2018).
[82] ATLAS, CMS Collaborations, Searches for gluinos and squarks, Proc. Sci. LHCP2019 (**2019**) 168 [arXiv:1909.11753].
[83] XENON Collaboration, Projected WIMP sensitivity of the XENONnT dark matter experiment, J. Cosmol. Astropart. Phys. 11 (2020) 031.
[84] Fermi-LAT Collaboration, Searching for Dark Matter Annihilation from Milky Way Dwarf Spheroidal Galaxies with Six Years of Fermi Large Area Telescope Data, Phys. Rev. Lett. **115**, 231301 (2015).
[85] Fermi-LAT, DES Collaborations, Search for gamma-ray emission from DES dwarf spheroidal galaxy candidates with Fermi-LAT data, Astrophys. J. Lett. **809**, L4 (2015).
[86] Y. Hiçyılmaz, M. Ceylan, A. Altas, L. Solmaz, and C. S. Un, Quasi Yukawa unification and fine-tuning in U(1) extended SSM, Phys. Rev. D **94**, 095001 (2016).
[87] ATLAS Collaboration, Search for high-mass dilepton resonances using 139 fb^{-1} of pp collision data collected at $\sqrt{s} = 13$ TeV with the ATLAS detector, Phys. Lett. B **796**, 68 (2019).
[88] CMS Collaboration, First constraints on invisible Higgs boson decays using $t\bar{t}H$ production at $\sqrt{s} = 13$ TeV, Report No. CMS-PAS-HIG-18-008, (2019).
[89] ATLAS Collaboration, Search for invisible Higgs boson decays in vector boson fusion at $\sqrt{s} = 13$ TeV with the ATLAS detector, Phys. Lett. B **793**, 499 (2019).
[90] CMS Collaboration, Search for invisible decays of a Higgs boson produced through vector boson fusion in proton-proton collisions at $\sqrt{s} = 13$ TeV, Phys. Lett. B **793**, 520 (2019).
[91] ATLAS Collaboration, Constraints on new phenomena via Higgs boson couplings and invisible decays with the ATLAS detector, J. High Energy Phys. 11 (2015) 206.
[92] CMS Collaboration, The CMS experiment at the CERN LHC, J. Instrum. **3**, S08004 (2008).
[93] CMS Collaboration, Searches for invisible decays of the Higgs boson in pp collisions at $\sqrt{s} = 7$, 8, and 13 TeV, J. High Energy Phys. 02 (2017) 135.
[94] W. Porod, SPHENO, a program for calculating supersymmetric spectra, SUSY particle decays and SUSY particle production at e^+e^- colliders, Comput. Phys. Commun. **153**, 275 (2003).
[95] W. Porod and F. Staub, SPHENO3.1: Extensions including flavour, CP-phases and models beyond the MSSM, Comput. Phys. Commun. **183**, 2458 (2012).
[96] M. D. Goodsell, K. Nickel, and F. Staub, Two-loop Higgs mass calculations in supersymmetric models beyond the MSSM with SARAH and SPHENO, Eur. Phys. J. C **75**, 32 (2015).
[97] F. Staub, SARAH 4: A tool for (not only SUSY) model builders, Comput. Phys. Commun. **185**, 1773 (2014).
[98] F. Staub, Exploring new models in all detail with SARAH, Adv. High Energy Phys. **2015**, 840780 (2015).
[99] J. Hisano, H. Murayama, and T. Yanagida, Nucleon decay in the minimal supersymmetric SU(5) grand unification, Nucl. Phys. **B402**, 46 (1993).

[100] Particle Data Group Collaboration, Review of particle physics, Chin. Phys. C **40**, 100001 (2016).

[101] ATLAS Collaboration, Observation of a new particle in the search for the Standard Model Higgs boson with the ATLAS detector at the LHC, Phys. Lett. B **716**, 1 (2012).

[102] P. Checchia *et al.* (ATLAS Collaboration), eds., Measurement of the Higgs boson mass in the $H \to ZZ^* \to 4\ell$ and $H \to \gamma\gamma$ channels with $\sqrt{s} = 13$ TeV pp collisions using the ATLAS detector, Phys. Lett. B **784**, 345 (2018).

[103] ATLAS Collaboration, Measurement of Higgs boson production in association with a $t\bar{t}$ pair in the diphoton decay channel using 139~ fb^{-1} of LHC data collected at $\sqrt{s} = 13$~ TeV by the ATLAS experiment, Report No. ATLAS-CONF-2019-004 (2019).

[104] ATLAS Collaboration, Combined measurement of differential and inclusive total cross sections in the $H \to \gamma\gamma$ and the $H \to ZZ^* \to 4\ell$ decay channels at $\sqrt{s} = 13$ TeV with the ATLAS detector, Phys. Lett. B **786**, 114 (2018).

[105] CMS Collaboration, Observation of a new boson at a mass of 125 GeV with the CMS experiment at the LHC, Phys. Lett. B **716**, 30 (2012).

[106] CMS Collaboration, Measurements of properties of the Higgs boson decaying into the four-lepton final state in pp collisions at $\sqrt{s} = 13$ TeV, J. High Energy Phys. 11 (2017) 047.

[107] CMS Collaboration, Search for a Higgs boson in the mass range from 145 to 1000 GeV decaying to a pair of W or Z bosons, J. High Energy Phys. 10 (2015) 144.

[108] CMS Collaboration, Measurement of Higgs boson production and properties in the WW decay channel with leptonic final states, J. High Energy Phys. 01 (2014) 096.

[109] ATLAS, CMS Collaborations, Measurements of the Higgs boson production and decay rates and constraints on its couplings from a combined ATLAS and CMS analysis of the LHC pp collision data at $\sqrt{s} = 7$ and 8 TeV, J. High Energy Phys. 08 (2016) 045.

[110] L. E. Ibanez and G. G. Ross, SU(2)-L × U(1) symmetry breaking as a radiative effect of supersymmetry breaking in guts, Phys. Lett. **110B**, 215 (1982).

[111] K. Inoue, A. Kakuto, H. Komatsu, and S. Takeshita, Aspects of grand unified models with softly broken supersymmetry, Prog. Theor. Phys. **68**, 927 (1982).

[112] L. E. Ibanez, Locally supersymmetric SU(5) grand unification, Phys. Lett. **118B**, 73 (1982).

[113] J. R. Ellis, D. V. Nanopoulos, and K. Tamvakis, Grand unification in simple supergravity, Phys. Lett. **121B**, 123 (1983).

[114] L. Alvarez-Gaume, J. Polchinski, and M. B. Wise, Minimal low-energy supergravity, Nucl. Phys. **B221**, 495 (1983).

[115] Heavy Flavor Averaging Group Collaboration, Averages of B-hadron, C-hadron, and tau-lepton properties as of early 2012, arXiv:1207.1158.

[116] LHCb Collaboration, First Evidence for the Decay $B_s^0 \to \mu^+\mu^-$, Phys. Rev. Lett. **110**, 021801 (2013).

[117] Heavy Flavor Averaging Group Collaboration, Averages of b-hadron, c-hadron, and τ-lepton properties, arXiv:1010.1589.

[118] Planck Collaboration, Planck 2018 results. VI. Cosmological parameters, Astron. Astrophys. **641**, A6 (2020).

[119] G. Bélanger, F. Boudjema, A. Goudelis, A. Pukhov, and B. Zaldivar, MICROMEGAS5.0: Freeze-in, Comput. Phys. Commun. **231**, 173 (2018).

[120] CMS Collaboration, Observation of a new boson with mass near 125 GeV in pp collisions at $\sqrt{s} = 7$ and 8 TeV, J. High Energy Phys. 06 (2013) 081.

[121] ATLAS Collaboration, Search for squarks and gluinos in final states with same-sign leptons and jets using 139 fb^{-1} of data collected with the ATLAS detector, J. High Energy Phys. 06 (2020) 046.

[122] T. Cohen, T. Golling, M. Hance, A. Henrichs, K. Howe, J. Loyal, Sanjay Padhi, and Jay G. Wacker, SUSY simplified models at 14, 33, and 100 TeV proton colliders, J. High Energy Phys. 04 (2014) 117.

[123] Z. Altın, Z. Kırca, T. Tanımak, and C. Salih Ün, Stop search in SUSY SO(10) GUTs with nonuniversal Gaugino masses, Eur. Phys. J. C **80**, 818 (2020).

[124] CMS Collaboration, Search for a Light Charged Higgs Boson Decaying to a W Boson and a CP-Odd Higgs Boson in Final States with e$\mu\mu$ or $\mu\mu\mu$ in Proton-Proton Collisions at $\sqrt{s} = 13$ TeV, Phys. Rev. Lett. **123**, 131802 (2019).

[125] CMS Collaboration, Search for resonances in the mass spectrum of muon pairs produced in association with b quark jets in proton-proton collisions at $\sqrt{s} = 8$ and 13 TeV, J. High Energy Phys. 11 (2018) 161.

[126] CMS Collaboration, Search for a light pseudoscalar Higgs boson produced in association with bottom quarks in pp collisions at $\sqrt{s} = 8$ TeV, J. High Energy Phys. 11 (2017) 010.

[127] CMS Collaboration, Search for an exotic decay of the Higgs boson to a pair of light pseudoscalars in the final state with two muons and two b quarks in pp collisions at 13 TeV, Phys. Lett. B **795**, 398 (2019).

[128] ATLAS Collaboration, Search for exotic decays of the Higgs boson into $b\bar{b}$ and missing transverse momentum in pp collisions at $\sqrt{s} = 13$ TeV with the ATLAS detector, J. High Energy Phys. 01 (2022) 063.

[129] D. Curtin *et al.*, Exotic decays of the 125 GeV Higgs boson, Phys. Rev. D **90**, 075004 (2014).

[130] J. Bernon, J. F. Gunion, Y. Jiang, and S. Kraml, Light Higgs bosons in two-Higgs-doublet models, Phys. Rev. D **91**, 075019 (2015).

[131] A. Cici, S. Khalil, B. Niş, and C. S. Un, The 28 GeV dimuon excess in lepton specific 2HDM, Nucl. Phys. B **977**, 115728 (2022).

[132] ATLAS Collaboration, Search for long-lived charginos based on a disappearing-track signature using 136 fb^{-1} of pp collisions at $\sqrt{s} = 13$ TeV with the ATLAS detector, Report No. ATLAS-CONF-2021-015 (2021).

[133] ATLAS Collaboration, Search for Displaced Leptons in $\sqrt{s} = 13$ TeV pp Collisions with the ATLAS Detector, Phys. Rev. Lett. **127**, 051802 (2021).

[134] H. Baer, I. Gogoladze, A. Mustafayev, S. Raza, and Q. Shafi, Sparticle mass spectra from SU(5) SUSY GUT models with $b - \tau$ Yukawa coupling unification, J. High Energy Phys. 03 (2012) 047.

[135] A. Delgado and M. Quirós, Higgsino dark matter in the MSSM, Phys. Rev. D **103**, 015024 (2021).

[136] XENON Collaboration, Dark Matter Search Results from a One Ton-Year Exposure of XENON1T, Phys. Rev. Lett. **121**, 111302 (2018).

[137] PandaX-II Collaboration, Dark Matter Results from 54-Ton-Day Exposure of PandaX-II Experiment, Phys. Rev. Lett. **119**, 181302 (2017).

[138] LUX Collaboration, Results from a Search for Dark Matter in the Complete LUX Exposure, Phys. Rev. Lett. **118**, 021303 (2017).

[139] DARWIN Collaboration, DARWIN: Towards the ultimate dark matter detector, J. Cosmol. Astropart. Phys. 11 (2016) 017.